University of Alberta

A Study of Interactions of Asphaltenes in Organic Solvents Using Surface Forces Apparatus

By

Jinggang Xie

A thesis submitted to the Faculty of Graduate Studies and Research

in partial fulfillment of the requirements for the degree of

Master of Science

in

Chemical Engineering

©Jinggang Xie

Edmonton, Alberta

Spring 2011

Abstract

A Surface Forces Apparatus (SFA) was used in this study to investigate the fundamental surface forces in oil sand processing research. Asphaltene coated surfaces were chosen as the research topic due to the critical role of asphaltenes in oil sands processing, from bitumen extraction, froth treatment to tailings treatment.

To mimic the real surface state in industry processing, dip-coated asphaltene surfaces were prepared for surface force experiments. In this study, a SFA 2000 was used to determine intermolecular and surface forces of asphaltene in organic solvents (toluene and heptane). The force vs. distance curves, or so-called force profiles obtained provide valuable information on local material properties such as interaction energies, molecular conformation changes of the interacting asphaltene surfaces or films. Atomic force microscopy (AFM) was used to provide complementary information on the surface morphology of the prepared asphaltene surfaces.

The results show that the surface interactions of asphaltenes strongly depend on types of surrounding solvents or vapours, contact time, load (pressure) and adsorption time to supporting substrate. Bridging adhesion forces were measured between one asphaltene surface and one mica surface in both pure toluene and heptane, as well as between two asphaltene surfaces in heptane. While small bridging adhesion was observed for two asphaltene surfaces in pure toluene, it changed to pure repulsion with increasing interaction time. The AFM imaging showed different degree of conformation and morphology changes with time of dip-coated asphaltene thin films in toluene and heptane,

which facilitated interpretations of the results from the SFA force measurements. The results obtained from this thesis study have provided an insight into the basic interactions and dynamic nature of asphaltenes in organic media and hence in crude oils and bitumen production.

This thesis is dedicated to my daughter Ellen,

for all the joys

and new meaning of life she has brought to us.

Table of Content

List of Tables

List of Figures

CHAPTER 1 INTRODUCTION

1.1 Oil Sands Industry

Oil Sands, also known as tar sands, have only recently been considered to be part of the world's oil reserves, as higher oil prices and new technology enable them to be profitably mined and upgraded to petroleum products. Oil sands are found in large amounts in many countries throughout the world, but are found in extremely large quantities in Canada and Venezuela. According to Government of Alberta, Canada's 180 billion barrels of proven oil reserves from oil sands (accounting for 15% of world reserves) rank the second largest after Saudi Arabia [Alberta ERCB, 2008]. The majority of these reserves, 170 billion barrels, are found in Alberta's oil sands. It is estimated that the oil sands deposit can secure Canada's energy supply for centuries to come.

Oil sands are essentially a mixture of bitumen, sands, clays and salty water. The principal value in oil sands is the bitumen, a viscous thick, sticky form of crude oil that will not flow unless heated or diluted with lighter hydrocarbons.

At present extracting bitumen from oil sands is the main business in Alberta. It is easy to get some of the bitumen out of the oil sands, but to get most out of them and minimize the environment impact are not easy. This is why we have to study the bitumen extraction process.

Canada is not the only one country that has oil sands resources, but it is the only one that has successfully mined the oil sands with mass production. The major reason for this commercial operation is that Alberta oil sands have a unique structure, different from those oil sands in Venezuela and State of Utah. In Alberta oil sands there is a very thin film of connate water between sands and the surrounding bitumen phase. The presence of this water film makes the water extraction process economical. In the mean time, people in Utah are struggling to develop solvent based extraction methods [DOE, 1985; Subramanian, 1996].

1.2 Water Based Bitumen Extraction

G.C. Hoffman of the Geological Survey of Canada is believed to be the first to separate bitumen from oil sand with the use of water in 1883. In 1913, Sidney Ells of the Federal Mines Branch began to test hot water flotation method of separating bitumen from oil sands. The bitumen produced was used to pave 600 feet of road in Edmonton that lasted for half a century. In the 1920's, entrepreneur R. C. Fitzsimmons applied the same hot water flotation process to produce bitumen for roofing and road surfacing at a plant near Bitumount, 80 kilometers north of Fort Mcmurray. Dr. Karl Clark, a scientist with the Alberta Research Council was granted a patent for the hot water extraction process in 1928 after extensive experimentation [Masliyah, 2007].

The hot water extraction process pioneered by Ells, Fitzsmmons and Clark proved to be the most economical method of extracting oil from oil sand over the years, although emerging in-situ technologies have been developed and put into practice.

Currently there are two commercial operation methods in oil sands production. One is the surface mining and the other is in-situ production. In-situ production may be SAGD (Steam Assisted Gravitation Drainage) or CSS (Cyclic Steam Stimulation) or the emerging VAPEX (Vapour Recovery Extraction) which utilizes solvents to separate the bitumen from the sand. For surface mining method, oil sands were shoveled and trucked to factories to be processed by hot water. For In-situ production process, bitumen is melted by piping hot steam or solvent down to oil sands formation, and pumped out directly from below the surface.

In a typical water based extraction process, there are essentially 5 steps [Drelich, 1994]:

1.   Bitumen film rupture

2.   Bubble formation on oil sand

3.   Bitumen attaching to or spreading over the gas bubble

4.   Rupture of bitumen bridges between sand grains

5.   Release of bitumen from sand and froth forming at the top of separation vessels

1.3 Bitumen Froth Treatment

After the gravitational separation and flotation extraction, the recovered bitumen froth typically consists of 60% bitumen, 30% water and 10% solids by weights. Solids and water need to be removed before sending the bitumen to the downstream upgrading facilities. Organic solvent such as Naphtha or Paraffin is used to dilute the viscous bitumen froth before centrifuge separation. If treated with paraffinic solvent, asphaltene will precipitate and separate out together with fine solids and water. Without the

problematic asphaltene in the bitumen, long distance hydrotransport of diluted bitumen is possible. Lower percentage of fines and water is more preferable in the downstream refinery facilities.

1.4 Surface Forces in Bitumen Extraction Process

In every step mentioned in bitumen extraction and froth treatment, interfacial interaction plays an important role. All these processes involve generation of new interface, increase or decrease of interfacial area. The evolvement of the shape and area is a collected result of a lot of forces from interaction phases. The governing theory for this process is interfacial science.

In interfacial science, we have interfacial tension, also called surface energy, which is a very good measure of how strong the interfacial force will be and how it will render the interfacial status.
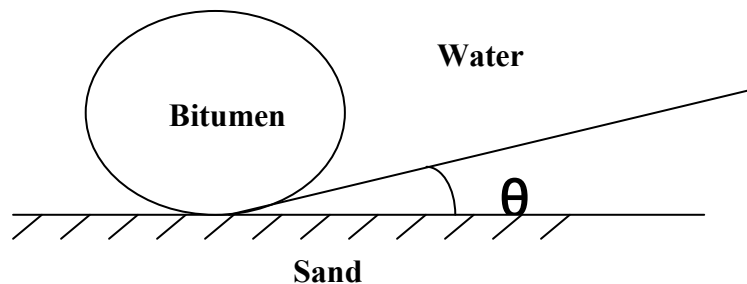
Figure 1.1 A bitumen drop sits on a sand surface in a water medium

For example, a bitumen drop sits on a solid surface in a water medium shown in Figure 1.1. The Young's equation can be used to depict this system in equilibrium:

$$\gamma_{BS} - \gamma_{SW} - \gamma_{BW} * \cos\theta = 0 \quad \text{or} \quad \cos\theta = (\gamma_{BS} - \gamma_{SW}) / \gamma_{BW} \qquad (1.1)$$

where γ_{BS}, γ_{SW} and γ_{BW} are the interfacial tensions between bitumen and solid, solid and water, and bitumen and water respectively. For a given system, the interfacial tensions of contacting phases determine a certain contact angle at equilibrium.

To pull off the two surfaces in Figure 1.1 from contact, a force greater than the adhesion force should be applied [Israelachvili, 1992]. The adhesion force is

$$F_{ad} = mR(\gamma_{BW} + \gamma_{SW} - \gamma_{BS}) \quad \text{or} \quad F_{ad} = mR\gamma_{BW}(1-\cos\theta) \qquad (1.2)$$

where R is the radius for the bitumen droplet and m is the coefficient with a value between π and 2π [Liu, 2005]. Interfacial tension is sufficient to depict the colloidal system at static state, but not convenient to prescribe the interfacial phenomena in a dynamic system. In the oil sands extraction process, bitumen, sands, and air bubbles, and water droplets are often mixeded together, forming a mixture of a lot of small particles in the slurry. This system is often called a colloidal system, because the dispersed particles normally have the size from nanometers to micrometers, and even to millimeters.

The particles are dispersed in the colloidal system, moving around because of the Brownian motion and hydrodynamic transportation. The interactions between them determine whether they will join together (coalesce or coagulate) or set apart (disperse), and what an equilibrium state (contact angle) will be, if attached to each other.

For example in bitumen extraction process, the bigger size the bitumen droplet, the higher bitumen recovery rate. To get bigger bitumen droplet, small bitumen droplets should be brought close and let join together. During this process, there will be interaction force between these two bitumen droplets. Actually this force is the so called surface force that determines the coagulation / coalescence behavior of bitumen droplets. The nature of the surface forces will be discussed in detail in Chapter 2. The adhesion force mentioned earlier is one special case of surface force when surfaces are pulled off.

1.5 Surface Forces Measurements

Since the surface force plays such an important role in bitumen extraction process, it is highly desirable to have a reliable measurement of it. The following plot shows an example of surface force profile between two colloid particles. Over the separation distance r, the force is always attractive, pulling two particles together. While the distance is below r, the force becomes more and more repulsive, resisting two particles to come too close.
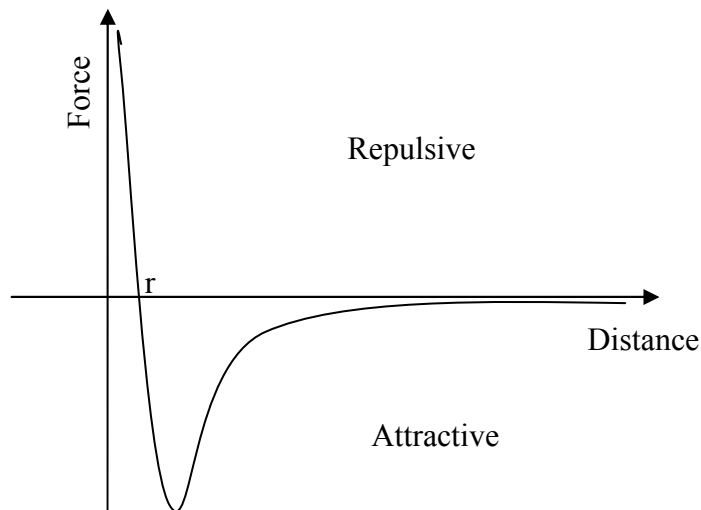
Figure 1.2 An example of force profile between two colloidal particles

As shown above, surface force profile shows the interactions between colloidal particles at different separations, from zero contact to hundreds of nanometers. It provides a whole image of colloidal system, acting as a key to understand the complicated interactions of mixed particles. Hence people also call the surface force profile as surface force law.

The surface force profiles obtained can greatly help to solve practical industry problems even though providing scientific explanations may still be difficult. This is why researchers in this field value measuring and understanding of surface forces fundamental.

Different surface force measurements provide different insights regarding the systems of interests. For example, some thermodynamic data on gases, liquids and solids (boiling point, PVT data) only provide thermodynamic information on the intermolecular force without giving any distance dependence [Israelachvili, 1992].

There are various methods to measure the surface force. For example the peeling experiment can give the adhesion force (a short range attractive force) of solid surfaces in contact. The measurement of surface tension and contact angle provide information on liquid-liquid and liquid-solid adhesion forces. The thickness measurement of soap film and liquid film adsorbed on surfaces can provide information on the long range repulsive forces stabilizing the liquid films [Israelachvili, 1992]. LeNeveu et al. [1976] developed an osmotic pressure technique to measure the collective interaction (disjoining pressure) of many small particles. Most of the above mentioned methods failed to give a force profile as a function of distance.

Wu et al. [1999] determined the colloidal force law between bitumen droplets by colloidal particle scattering method, a technique based on calculating colloidal forces from droplet-droplet collision trajectories. This is a measurement of the surface force as a function of separation distance although the force is not directly measured.

Ideally, it will be unambiguous if one can just directly measure the surface force between two colloidal particles. In fact, it is not easy to directly measure the forces between two small colloidal particles by any conventional method, because the surface forces can be as small as 10^{-15} N. It is not even possible to get hold of a small colloidal particle by any means.

Fortunately Derjaguin solved this dilemma by his famous approximation, "Derjaguin Approximation", named after his name [Israelachvili, 1992; Butt, 2003]. In Derjaguin approximation, one can relate the surface forces between two curved shapes to the surface force between two flat surfaces [Israelachvili, 1992; Hunter, 2001]. Hence the surface forces between many different shapes of bodies can be related to each other by the Derjaguin approximation.

For example, it is difficult to directly measure the surface forces between two small colloidal particles of micrometer sizes. But one can measure the surface force between two bigger particles of centimeter sizes. With the Derjaguin approximation, the direct surface force measurements between larger size surfaces can provide useful force law in colloidal world.

To directly measure the surface force, currently there are mainly two techniques. One is AFM (Atomic Force Microscope) [Ducker, 1991; Ducker, 1992]. The other one is SFA (Surface Force Apparatus)[Israelachvili, 1992].

In the oil sands extraction lab at University of Alberta, extensive research on surface force measurement has been carried out using AFM technique [Liu, 2004; Long, 2006; Zhao, 2006 and Wang, 2009]. A lot of very valuable research results have been obtained with the AFM. In AFM force measurement, the absolute separation between two surfaces is not measured directly. For some soft and deformable surfaces the separation obtained by AFM force measurement might not be very accurate.

Asphaltene is commonly defined as the molecular fraction in crude oil or bitumen that is soluble in toluene but insoluble in n-heptane. Asphaltene is very sensitive to the environment[Mullins, 2007]. A small change in solvent composition, temperature and pressure may lead to asphaltene aggregation or precipitation in pipeline or container.

Vuillaume et. al. [2009] applied the SFA technique to measure the interactions between mica surfaces across crude oil and asphaltene solutions from Campos Basin, Brasil. To have better understanding of asphaltenes involved surface interactions in oil sands industry, some pioneer research work in this field has been carried out with AFM colloidal force technique[Liu, 2003; Wang, 2009].

In this study, an SFA 2000 was used to study the asphaltene surface interactions. By coating asphaltene films on mica surfaces, the symmetric and asymmetric interactions between the asphaltene surfaces or mica surfaces in toluene and heptane were determined. The force vs. distance curves, or so-called force profiles, have provided valuable information on local material properties such as interaction energies, and molecular conformation changes of the interacting asphaltene surfaces or films. Atomic force microscopy (AFM) was used to provide complementary information on the surface morphology of the asphaltene films studied.

CHAPTER 2 SURFACE FORCES IN OIL SANDS INDUSTRY

2.1 Surface Forces

The surface force is the force acting on the colloidal surfaces in the distance range within several hundreds nanometers. It is the surface force that determines how bitumen attaches to the sand and how stable small water droplets can be in the final bitumen products. Actually the surface force is the core of colloidal science. For a long time, people noticed the colloidal phenomena and found some facts or raw experiences in the colloidal world. But only after the DLVO (Derjaguin and Landau of the USSR, and Vervey and Overbeek of the Netherland) theory was proposed in 1940's, the colloidal research became real science [Israelachvili, 1992; Hunter, 2001; Masliyah, 2006; Butt, 2003]. In DLVO theory, the surface force is divided into two components: the van der Waals forces (F_{vdw}) and the electric double layer forces (F_E). The total surface force is the collective effect of the two:

$$F = F_{vdw} + F_E \qquad (2.1)$$

The modern science has put all the forces in the universe into four categories, i.e. the four fundamental forces, according to their originations. The strong and weak forces act only at very short distances less than 10^{-5} nm, and are responsible for holding certain nucleons and compounding nuclei together. The gravitational force acts between masses and the electromagnetic force acts between electric charges.

Both the van der Waals forces and the electric double layer forces belong to the category of the electromagnetic force.

2.1.1 van der Waals forces

A lot of molecules make up a colloidal particle. Within molecules, there are permanent dipoles and induced transient dipoles. Electromagnetic forces between these dipoles are the source of van der Waals forces. Van der Waals forces (F_{vdw}) consist of three distinct contributions:

1. Orientation force, the electrostatic interactions between permanent dipoles. This electrostatic interaction is sometimes called Keesom interaction or Keesom force (F_{Keesom}) after Willem Hendrik Keesom.

2. The second source of attraction is induction (also known as polarization), which is the interaction between a permanent dipole on one molecule with an induced dipole on another. This interaction is also called Debye force (F_{Debye}) and sometimes measured in debyes after Peter J.W. Debye.

3. The third attraction, London force (F_{London}) is named after Fritz London who himself called it dispersion force. This is the only attraction experienced by non-polar atoms. It is operative between any pair of molecules, irrespective of their symmetry.

The van der Waals forces are the sum of Keesom force, Debye force and London force, while for most cases the London force is dominating.

$$F_{vdw} = F_{Keesom} + F_{Debye} + F_{London} \qquad (2.2)$$

Because of the similar origin, the three terms contain the same distance dependency. The potential energy for the three interactions all decreases with $1/D^6$. The van der Waals

interaction energy between Molecular A and Molecular B, $W_{AB}(D)$ can be expressed in the following equation:

$$W_{AB}(D) = - C_{AB} / D^6 \qquad\qquad (2.3)$$

where C_{AB} is a constant depending on different types of molecules. The van der Waals forces between the molecules within the particle are inner forces, which makes no contribution to the interactions between particles. The molecules in one particle exert forces to the molecules in another particle, causing the intermolecular van der Waals forces across the particles. The van der Waals forces between two bodies are nothing but collectively the sum of all the intermolecular van der Waals forces. It is actually a body force, because it accounts for the forces between all the molecules, from surface to the core, in both particles. Since the interaction potential decay dependency is D^{-6}, the forces from the thin layers facing to other particle contribute to nearly the whole van der Waals force, while other forces by the bulk molecules is almost negligible because of bigger D values compared with those of thin layers facing to other particles . This is why we refer the colloidal force as surface force. Indeed it is the surface molecules that determine the surface force and hence interfacial properties.

Based on the concept that the van der Waals forces between two macroscopic bodies are the summation of intermolecular van der Waals forces, there are two ways, i.e. the microscopic approach and macroscopic approach, to calculate the total macroscopic van der Waals forces [Israelachvili, 1992]. Fortunately these two approaches lead to similar results as summarized below.

The van der Waals interaction energy decreases with $1/D^6$ between molecules. Between two macroscopic bodies the decay is less steep and it depends on the specific shape of the interacting bodies. For two infinitely extended plates separated by a gap of a thickness D the van der Waals energy per unit area W is:

$$W = -\frac{A_H}{12\pi D^2} \tag{2.4}$$

where A_H is the Hamaker constant determined by the dielectric permittivities and the optical properties of the interacting media [Butt, 2003; Israelachvili, 1992]. Hamaker constant is related to surface energy by the following equation:

$$\gamma_s = \frac{A_H}{24\pi D_0^2} \tag{2.5}$$

where γ_S is the surface energy or interfacial tension of the solid, D_0 is the distance between two bulk atoms in the solid.

According to Lifshitz's theory, the combined Hamaker constant can be calculated from the dielectric permittivities and the optical properties of the interacting media [Israelachvili, 1992]. The following is the expression of non-retarded Hamaker constant for two macroscopic phases 1 and 2 interacting across a medium 3, A_{Total}:

$$
A_{Total} = A_{v=0} + A_{v>0}
$$
$$
\approx \frac{3}{4}kT\left(\frac{\varepsilon_1 - \varepsilon_3}{\varepsilon_1 + \varepsilon_3}\right)\left(\frac{\varepsilon_2 - \varepsilon_3}{\varepsilon_2 + \varepsilon_3}\right) + \frac{3h\nu_e}{8\sqrt{2}}\frac{(n_1^2 - n_3^2)(n_2^2 - n_3^2)}{(n_1^2 + n_3^2)^{\frac{1}{2}}(n_2^2 + n_3^2)^{\frac{1}{2}}\left[(n_1^2 + n_3^2)^{\frac{1}{2}} + (n_2^2 + n_3^2)^{\frac{1}{2}}\right]}
$$

(2.6)

where $A_{v=0}$ and $A_{v>0}$ are the contribution to Hamaker constant for v equals 0 and greater than 0, respectively, k is the Boltzmann constant, T is the temperature, ε is the dielectric permittivity of media, h is Planck constant, v_e is the main electronic absorption frequency in the UV regime, typically 3×10^{15} s^{-1} and n is the refractive index of the medium in the visible range.
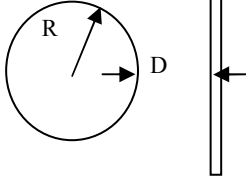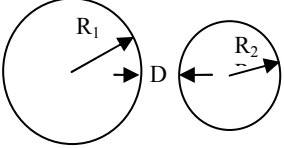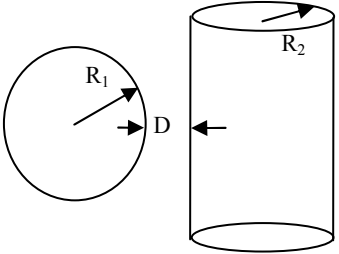
2.1.2 Derjaguin approximation

The van der Waals forces between two infinitely extended flat plates can be easily calculated. A real colloidal system often involves many colloidal shapes other than extended plates. The Derjaguin approximation relates the interaction between two bodies of arbitrary shapes at distance D to the energy per unit area between two planar surfaces W(D), as long as the range of the interaction and the separation D is much less than the curvature radius of the surfaces.

Figure 2.1 shows the van der Waals interaction forces between several geometries [Hunter, 2001].

The Derjaguin approximation applies to general forces including vdw forces and electrostatic double layer forces to be introduced later on.

Table 2.1 van der Waals interaction forces between several geometries

	Between a sphere and an infinite plate $\quad F(D) = -2\pi R W(D)$ $\qquad\qquad$ (2.7)
	Between two spheres $\quad F(D) = -2\pi(R_1 R_2/(R_1+R_2))W(D)$ $\qquad$ (2.8)
	Between two cross cylinders $\quad F(D) = -2\pi(R_1 R_2)^{0.5}W(D)$ $\qquad$ (2.9)

2.1.3 Electrical double layer and double layer forces

When surfaces are immersed in electrolyte solutions, usually there will be charges on their surfaces. For example, in the oil sand extraction process, particles in oil sand slurry carry static charges on their surfaces. Montmorillonite clay will carry negative charge in water at its basal plane, positive or negative charge at edges, depending on the pH [Masliyah, 2007]. Bitumen will normally carry negative charge because of the natural surfactants at the interface. Air bubbles could also be negatively charged by the natural surfactants [Masliyah, 2007].

All the charges are on the surfaces of particles. The charges on the surfaces create an electric field in the liquid phase. The electric field can attract counter ions, which are normally present in electrolyte solutions. The surface charges and the attracted counter ions form the electrical double layer structure. The concept of electrical double layer was first proposed by Helmohotz [Butt, 2003]. In the simplest Helmohotz model, the counter ions bind directly to the surface and neutralize the surface charge like a plate capacitor.

In the 1910's, Gouy and Chapman proposed a diffusion double layer model by taking into account a thermal motion of the ions and assuming the ions have no volume. The thermal fluctuations drive the counter ions away from the surface where Poisson-Boltzmann distribution of the counter ions can apply.

Gouy and Chapman theory makes a lot of assumptions,e.g., the finite size of the ions is negligible, solvent is continuous, and surfaces are molecularly flat.

Stern (1924) and Grahame [1947] combined the ideas of Helmholtz with that of Gouy and Chapman by developing a modern electric double layer theory. In the Stern-Grahame theory the double layer is divided into two parts: an inner part, the Stern layer, and an outer part, the diffuse layer. The stern layer is an immobile layer of adsorbed counter ions. The outer boundary of the Stern layer is shear plane because ions become mobile outside that plane. Outside the Stern layer the mobile ions obey the Poison-Boltzmann distribution. The potential at the shear plane is called zeta potential or shear potential.

For negatively charged surfaces in solution, a Stern-Grahame model is depicted in Figure 2.1
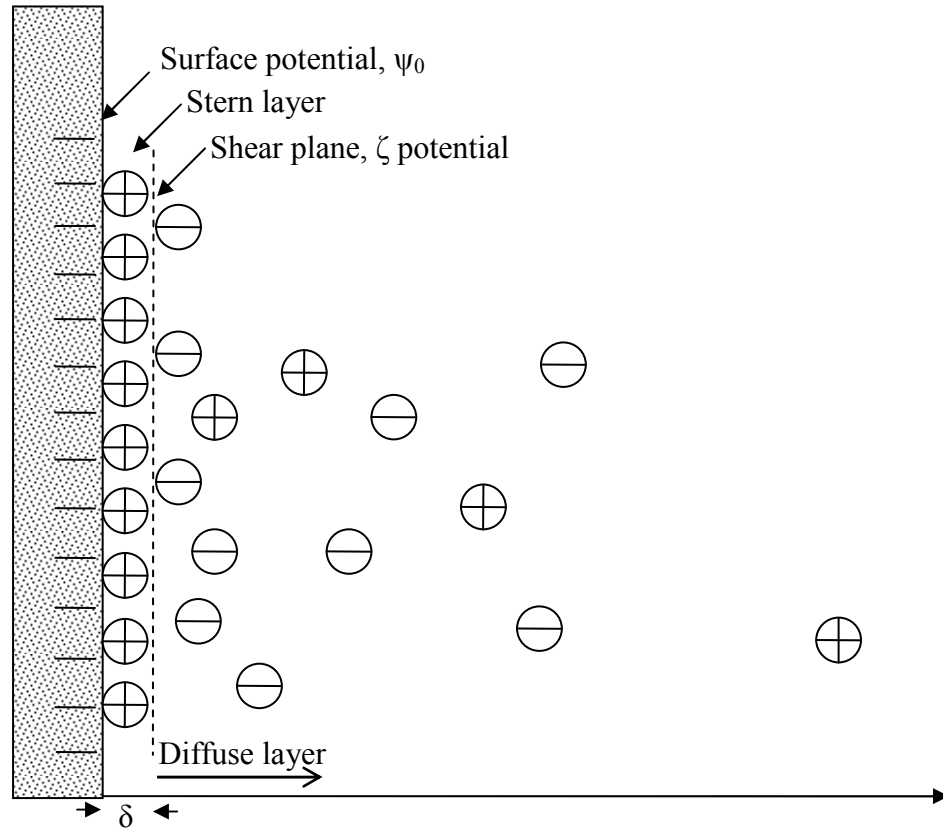
Figure 2.1 Stern-Grahame model for negatively charged surfaces in solution

The electric field created by the double layer causes potential gradient in the electrolyte solutions. The mobile ions in the diffuse layer obey the Boltzmann distribution. Charge density (ρ_e) and electric potential (ψ) are related by Poisson equation:

$$\nabla^2\psi = \frac{\partial^2\psi}{\partial x^2} + \frac{\partial^2\psi}{\partial y^2} + \frac{\partial^2\psi}{\partial z^2} = -\frac{\rho_e}{\varepsilon\varepsilon_0} \tag{2.10}$$

For flat, infinite and uniform surfaces, the above equation can be simplified to one dimension.
$$\nabla^2\psi = \frac{d^2\psi}{dx^2} = -\frac{\rho_e}{\varepsilon\varepsilon_0}$$

$$(2.11)$$

where x is the distance to the surface, ψ is the local electric potential in the electrolyte solutions, ρ_e is the local charge density in the solution, ε is relative dielectric permittivity and ε_0 is the permittivity of vacuum.

Boltzmann distribution predicts the distribution function for the fractional number of particles occupying a set of states which each respectively possess different energy. The following Figure 2.2 shows the ions distribution near a positively charged surface. n_0 is the bulk concentration of the single symmetric electrolyte, and n_+, n_- are the local concentrations of cations and anions respectively.
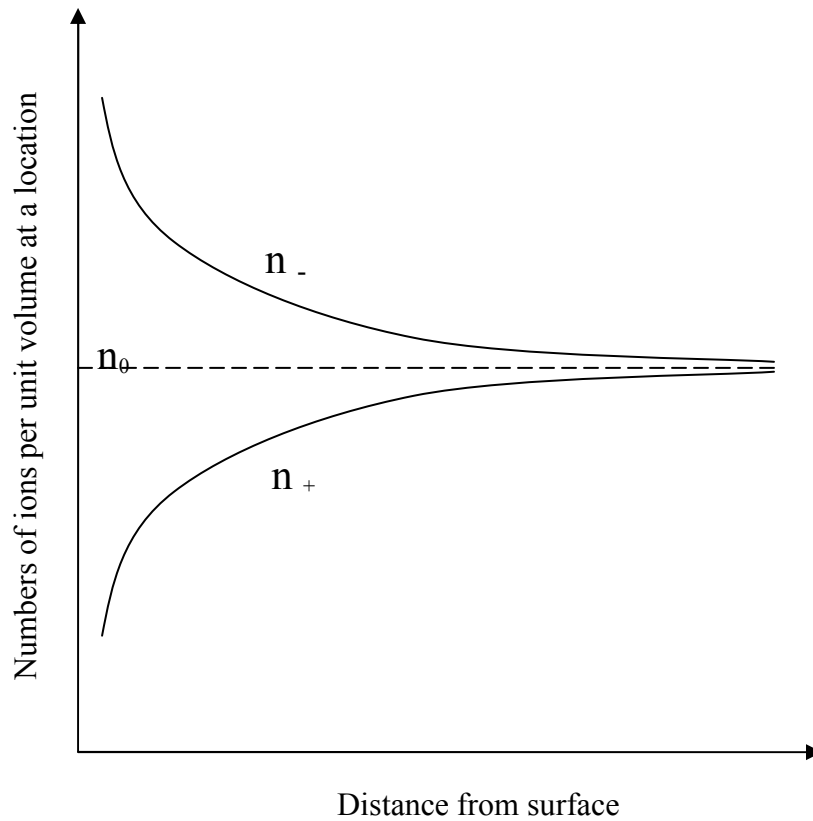
Figure 2.2 Boltzman distribution of ions near a positively charged surface

If the local electric potential is ψ, and the electrolyte is single symmetrical the numbers of ions per unit volume at different local electric potential will be:

$$n_+ = n_0 \exp\left[\frac{-ze\psi}{kT}\right]$$ (2.12a)

$$n_- = n_0 \exp\left[\frac{ze\psi}{kT}\right]$$ (2.12b)

So the overall charge density ρ_e is:

$$\rho_e = ze(n_+ - n_-) = zen_0\left\{\exp\left[-\frac{ze\psi}{kT}\right] - \exp\left[\frac{ze\psi}{kT}\right]\right\} = -2zen_0 \sinh\left[\frac{ze\psi}{kT}\right]$$ (2.13)

where e is the constant of elementary charge, and z is 1 for single charged ions.

Combining Poisson's equation with Boltzmann distributions, we get a differential equation as below:

$$\frac{d^2\psi}{d\,x^2} = \frac{2zen_0}{\varepsilon\varepsilon_0} \sinh\left[\frac{ze\psi}{kT}\right]$$ (2.14)

With two boundary conditions, this differential equation can be solved. The electric potential distribution is impacted by the electrolyte type and concentration, and the temperature. For example, if the boundary condition is for constant surface potential:

$$\psi = \psi_0 \ \text{ at } x = 0;$$

$$\psi = 0 \ \text{ at } x = \infty$$

The electric potential distribution is determined by the following equation:

$$\psi = \frac{2kT}{ze} \ln\left[\frac{1+\delta\exp(-\kappa x)}{1-\delta\exp(-\kappa x)}\right] \tag{2.15}$$

where $\kappa = (\sum_i n_{i0}e^2 z_i^2 / \varepsilon\varepsilon_0 kT)^{1/2}$, and $\delta = \tanh(ze\psi_0/4kT)$

The Debye length $1/\kappa$ is the characteristic decay length of the potential.

For $\frac{ze\psi_0}{2kT} \langle\langle 1$, Debye-Huckel approximation applies, the electric potential decays exponentially in the double layer from surface to the bulk:

$$\psi = \psi_0 \exp(-\kappa x) \tag{2.16}$$

If two charged surfaces approach each other and the electric double layers overlap, an electric double layer force arises, as shown in Figure 2.3. It can be repulsive or attractive depending on the sign of the surface charges. The nature of the force is electromagnetic force while the origin of the force is the osmosis pressure because there are extra or less ions in the gap than in the bulk.
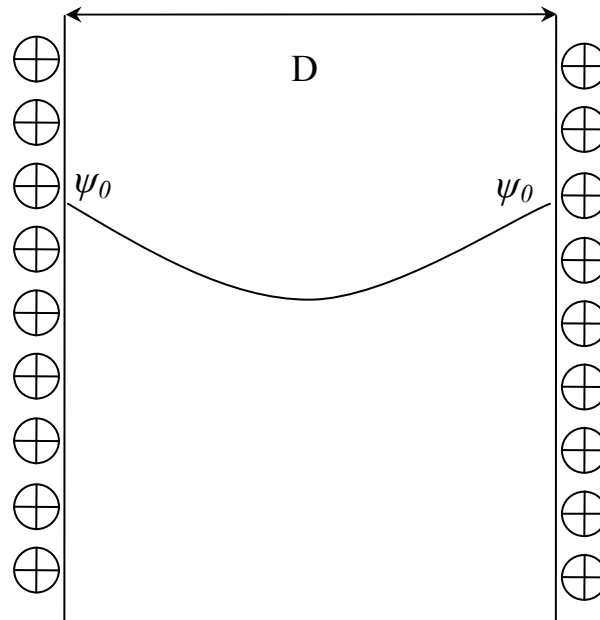
Figure 2.3 Overlapped double layers between two charged surfaces

in electrolyte solution

For two surfaces with the same surface potential ψ_0, and in z:z symmetric electrolyte, the double layer interaction free energy per unit area between two infinite flat surfaces at distance D can be expressed as following:

$$W(D) = (64kTn_0\gamma^2 / \kappa)\exp(-\kappa D) \tag{2.17}$$

According to the Derjaguin approximation, the double layer interaction between two spheres with radius R can be expressed as:

$$F = -\pi RW(D) \tag{2.18}$$

By integration the above F over the distance from infinity to D, the double layer interaction free energy per unit area between two spheres at distance D can be expressed as following:

$$E(D) = (64\pi kTn_0 R\gamma^2 / \kappa^2)\exp(-\kappa D) \tag{2.19}$$

Similarly, the double layer interaction between two crossed cylinders with radius R can be expressed as:

$$E(D) = (128\pi kTn_0 R\gamma^2 / \kappa^2)\exp(-\kappa D) \tag{2.20}$$

It clearly shows that the double layer interaction between two surfaces, regardless of the geometries, decays exponentially with distance. The characteristic decay length is the Debye length.

In practical application, the ζ potential is used as the surface potential. In fact, the surface potential decays from the shear plane where the local potential is ζ potential by approximation.

2.2 DLVO Theory

It was Derjaguin, Landau, Vervey and Overbeek who first built the concept that the colloidal forces are the combination of the van der Waals forces and electrostatic force [Derjaguin and Landau, 1941; Vervey and Overbeek, 1948]. Their theory is now called DLVO theory, which is the foundation of modern colloidal science.

The DLVO theory considers the van der waals forces and double layer force at the same time. For example, the DLVO forces for two flat and infinite extended surfaces with the same surface potential ψ_0 in z:z symmetric electrolyte can be expressed as below:

$$F_{DLVO} = F_{vdw} + F_E = -\frac{A_H}{6\pi D^3} + (64kTn_0\gamma^2)\exp(-\kappa D) \tag{2.21}$$

Or in the energy form, the equation can be put as :

$$W_{DLVO} = W_{vdw} + W_E = -\frac{A_H}{12\pi D^2} + (64kTn_0\gamma^2/\kappa)\exp(-\kappa D) \tag{2.22}$$

The overall effect of the DLVO forces depends on the separation, D. By plotting the W_{DLVO} vs the separation D, one can easily assess the stability of the colloidal system.

The DLVO theory has been very successful in interpreting the aqueous inorganic colloidal system where the double layer system is well developed and the surface condition is relatively simple. In this thesis the DLVO forces were not measured due to the organic solvents used. However, it would be helpful to review the DLVO forces here because non-DLVO forces are referenced with DLVO forces.

2.3 Non-DLVO Forces and Extended DLVO Theory

For organic solvent or some polymer related surfaces, there are more forces besides the DLVO forces present in the colloidal system. Considering only the DLVO forces, misleading results may occur. There are forces like hydrophobic forces, hydration forces, steric forces etc. introduced into the colloidal science[Israelachvili, 1982; Pashley, 1981; Klein, 1982]. Generally, they were categorized as non-DLVO forces. The origins of non-DLVO forces are so rich that not all of them are fully understood. The DLVO theory has then been developed to the extended-DLVO theory to depict the force behavior of the colloidal system (Butt, 2003 and Masliyah, 2006). Sometimes the non-DLVO forces can play significant roles in bitumen extraction process[Liu, 2004].

Hydrophobic interaction is one of the most important non-DLVO forces. In 1982, the hydrophobic force was directly measured for the first time [Israelachvili, 1982]. After several decades research on types of hydrophobic surfaces, the magnitude and distance dependency of hydrophobic interaction remain unclear. But the short range attraction represents the "true" hydrophobic interaction because it is the only one can be seen for all surfaces [Lin, 2005].

Hydration forces were originally proposed by Langmuir etc. to account for the repulsion and swelling of amphiphilic and colloidal surfaces even when there is no electrostatic repulsion between them. These forces are believed to arise whenever surfaces are hydrophilic. It is a strong short-range, typical range of 1-3 nm, repulsive force. Below

this range they can dominate over the van der Waals and electrostatic double-layer forces[Israelachvili, 1990].

For some surfaces with protruding brushes, steric forces are often found. The brush may be the polymer attached to the surface or surfactant adsorbed. It may be attractive or repulsive depending on conditions such as solvent environment [Liu, 2004].

Different models accounting for the contributions of the non-DLVO forces have resulted in the extended DLVO theory. Hence a lot of force measurements can be explained with better scientific basis, although it is far from total understanding of these surface forces.

Surface forces have different sources. But in the direct force measurement, we can not tell which part of the force belonging to van der Waals force, and which part to electrostatic force. Only after we do the force profile data analysis, such as data fitting, can we attribute these factors to different sources (Masliyah, 2006).

As introduced in Chapter 1, surface forces play an important role in the oil sand extraction process. In this thesis, Surface Force Apparatus will be used to measure the surface forces. More specifically, asphaltene-asphaltene interactions in organic solvent will be examined.

CHAPTER 3   DIRECT SURFACE FORCE MEASUREMENT

Surface Force Apparatus (SFA)

3.1 The Surface Force Apparatus (SFA) and SFA Attachments

Surface force apparatus was developed by Israelachvili et.al. from Derjaguin and his coworkers' prototype measurement of van der Waals forces between a convex lens and a flat glass surface in vacuum [Israelachvili, 1992]. Israelachvili's SFA measures surface forces between two cross cylinder surfaces. For the convenience of assembly, round disks with one face polished into cylindrically curved surface are used in SFA. The crossed-cylinder geometry (of same radius R) roughly corresponds to a sphere of radius R approaching a flat surface, based on the Derjaguin approximation: $F(D) = -2\pi RW(D)$, where $F(D)$ is the force between the two curved surfaces and $W(D)$ is the interaction energy per unit area between two flat surfaces.
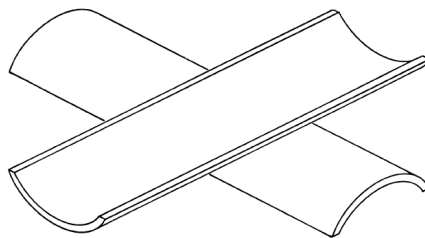
Figure 3.1: Cross placed cylindrical surfaces in SFA experiment

The current SFA can measure the surface forces in various liquid media and vapors, even opaque medium with a separation accuracy down to 1 Å. Because the separation is measured directly by FECO (Fringes of Equal Chromatic Order) technique, an optical interference method, deformation of the surface has almost no impact on the final separation measurement [Israelachvili,1973]. The real surface curvature can be determined during the force measurements in real time, and this gives SFA an advantage over AFM technique especially when soft surfaces are involved.

Figure 3.2 serves as a simple but clear description of force measurement principle used in the SFA. Two disks with crossed cylindrical surfaces are held center to center by a piezoelectric scanner and a force spring, respectively. When the surfaces are set far away from the surface force interaction distance, the surface force is zero. The force spring is at its initial state and the piezoelectric scanner is stretched from its initial length S_0. By optical interference FECO method, the absolute distance between the two surfaces is determined as D_0.

When applying certain voltages on the piezoelectric scanner, it will stretch out and push the upper surface towards the lower surface. Meanwhile, the separation between two surfaces will be reduced. When the separation is reduced into the surface force interaction range, the lower surface may be pushed downwards if the surface force is repulsive or be attracted upwards if the surface force is attractive. Figure 3.2 depicts the case of repulsive surface force.

From the initial zero force state to the non-zero force state, the piezoelectric scanner stretching distance is $\Delta D_{applied}$, which is controlled with accuracy of 1 Å by controlling voltages on the piezoelectric scanner with accuracy of 0.1 Volt. The voltage-distance relation of the piezoelectric scanner needs to be predetermined before each force measurement as it may change with different experiment environments.

From the initial zero surface force state to the non-zero force state, the absolute separation between surfaces changed from D_0 to D. They are both measured by FECO technique with the accuracy of 1 Å. The actual distance that surfaces move relative to each other is $\Delta D_{meas} = D_0 - D$.

With the spring constant k predetermined, the surface force F is ready to be obtained by measuring the spring displacement x from zero force state to interaction state:

$$F(D) = kx$$

The spring displacement x is nothing but the difference of $D_{applied}$, the moving distance of the piezoelectric scanner and ΔD_{meas}, the actual distance that surfaces move relative to each other:

$$x = \Delta D_{applied} - \Delta D_{meas}$$

Hence

$$F(D) = k(\Delta D_{applied} - \Delta D_{meas})$$
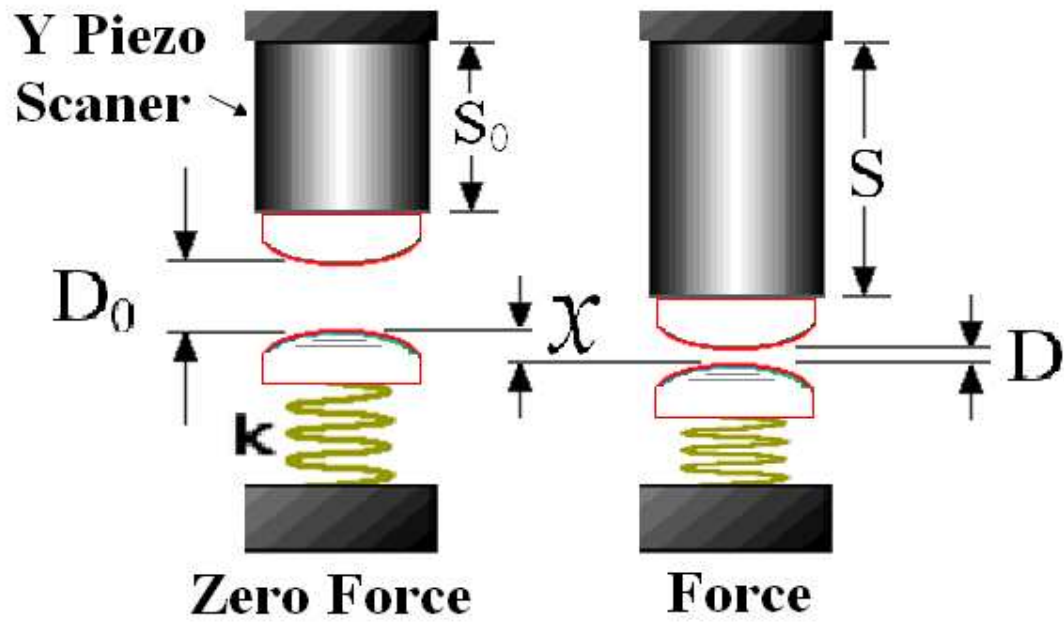
$$\Delta D_{applied} = S - S_0$$

$$\Delta D_{meas} = D_0 - D$$

$$F(D) = k(\Delta D_{applied} - \Delta D_{meas}) = kx$$

Figure 3.2: Simple description of the mechanism of the normal force measurement of SFA

The SFA 2000 we used was purchased from Surforce Company at Santa Barbara, USA. It is the newest version of SFA developed by Professor Israelachvili et.al, and is aimed for a wider scope of users both from academy and industry. The SFA 2000 is schematically shown in Figure 3.3. The main components are the main chamber, the micrometers, the main stage containing the central single-cantilever spring, the lower disk holder and the upper disk holder on the piezoelectric scanner. The upper surface sample is located on the central hole of the piezoelectric scanner, and the lower surface sample is mounted on the end of the flat spring cantilever. During SFA experiments, the surfaces are brought together or separated at different levels by four main controls, i.e. the course manual micrometer, fine manual differential micrometer, motor driven micrometer and piezoelectric scanner. The forces between the surfaces are measured by the deflection of a flat spring cantilever. In SFA, surface forces between the two surfaces on the order of 10 nN can be measured.

The crucial element of the SFA 2000 is the short single-cantilever spring on the Main Stage. The main feature of the single-cantilever on the main stage is that it can translate the movement of the micrometers into the movement of surfaces with a reducing factor up to 1000.

One turn of the coarse manual micrometer head corresponds to 0.5 mm displacement of the surfaces, and the total movement of the lower surface can be 2 mm from the coarse

manual micrometer. One turn of the fine manual differential micrometer head provides 70 μm surface movement. The fine manual micrometer gives the total movement of the lower surface 200 μm .The motor driven micrometer can move the surface up to 10 μm while the motor itself has a moving range of 10 mm. The surface position accuracy by the motor driven micrometer is within 0.2 nm. The piezoelectric scanner is the only control to move the upper surface. It can control the surface movement at the accuracy of 0.1 nm with a total moving range of 1 μm.

One can manipulate the movement of the surfaces by the four levels of control mentioned above. But during force measurement, only motor driven micrometer and piezoelectric scanner can provide desired level/resolution of surface displacement. The details on operations of SFA 2000 can be found in the following PhD thesis [Meyer, 2006; Alig, 2007; Zeng, 2007].
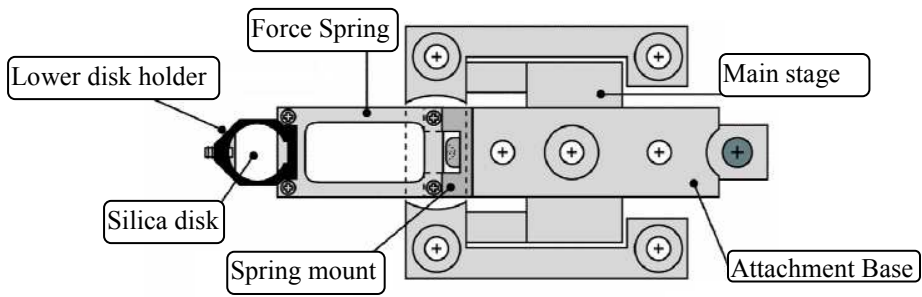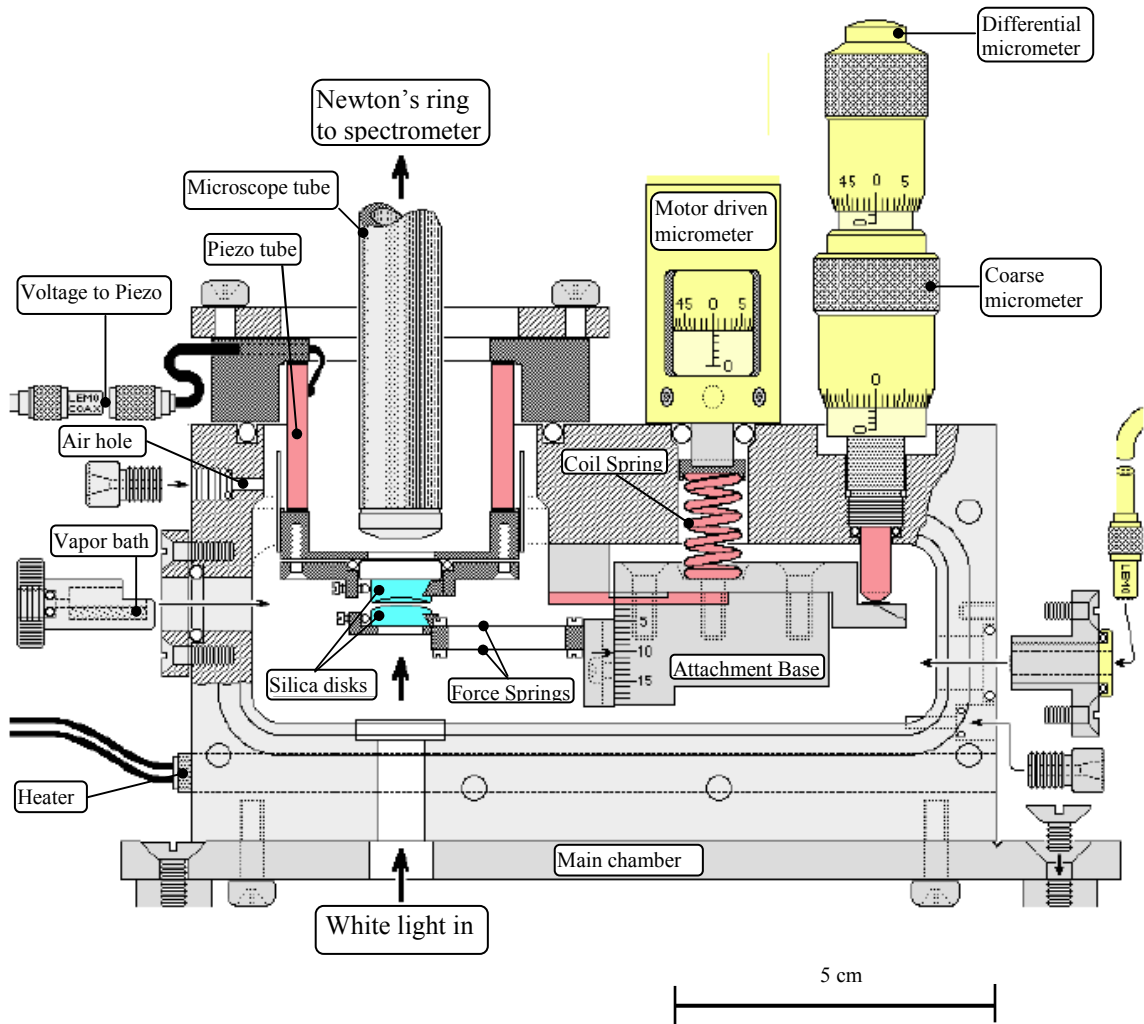
Figure 3.3: Detailed schematics of the SFA 2000 with the main components in place in the main chamber (top) and top view of the main stage and the force cantilever (bottom)

3.2 Preparation of Surfaces

Fresh cleaved transparent mica sheet are molecularly smooth surfaces [Israelachvili, 2004], which are commonly used in SFA experiments as interaction surfaces or supporting substrates. Other types of surfaces such as sapphire had also been used [Israelachvili, 1992]. Preparation of SFA surfaces often involves cleaving of mica sheets, silver coating on mica sheets, gluing of mica to silica disk, and further treatment of the surfaces.

3.2.1 Cleaving of mica sheets

Mica peeling, gluing and mounting are carried out in a dust free laminar flow cabinet. Powder free gloves should be worn in order to prevent contamination from hand to fresh mica surfaces. It is highly advisable to wear personal protection equipment to avoid inhalation of fine mica flakes.

The crystalline structure of mica forms layers that can be split or delaminated into thin sheets. Molecularly smooth surface can be obtained by peeling through its layer structure. Chemically, mica is a complex hydrous aluminum silicate, containing potassium and traces of other elements. Mica is stable when exposed to electricity, light and extreme temperatures and inert to water, acids (except hydrofluoric and concentrated sulfuric acids), alkalis, conventional solvents and oil.

In this study natural Ruby Muscovite mica, $KAl_2(AlSi_3O_{10})(OH)_2$, was purchased from S&J Inc., USA. It is considered of higher quality (compared to green muscovite) because of hardness and excellent cleavage properties, permitting it to be split into the thinnest film without the risk of cracking. Mica is optically flat, resilient and incompressible. While mica splits into thin films along its cleavage planes, mica surface remains tough.

Cleaving mica involves insertion of a sharp edge or point into an edge or corner of the mica sheet and prying against its van der Waals forces between its layers. Sharp tweezers with tip end less than 10 μm can be used for mica cleaving. A large and thick mica sheet is selected before trimming its edges with scissors (Figure 3.4, a). Clean of all excess flakes on the mica before inserting a sharp needle into the edge of the thick sheets (Figure 3.4, b). With gentle moving of the needle along the cracking gap, two pieces of mica sheet can be obtained. The mica sheets can be held by hands at the edges, but the center fresh mica surfaces should not be touched or contaminated. Under the neon light of the laminar flow cabinet, one can examine the fresh mica surfaces. Steps can be seen at a certain observing direction. One should keep peeling the mica sheet until a mica sheet step free on the central area is obtained (Figure 3.4, c). This sheet can be treated as "back sheet" for storing thinner mica films. Thinner mica film is obtained by further peeling from the other sheet. As the thickness goes to the order of μm, colors from light interference can appear on the surface under the neon light. When the thickness is over 10 μm, it is white. Then it goes from green to yellow, and from yellow to red when it becomes thinner and thinner. Those colors change abruptly at cleavage steps, but remain uniform over regions of constant thickness. Thin mica film flaps along the air flow in the

laminar flow cabinet. It is usually advisable to peel the thin film from the thick sheet at a uniform rate of about 5mm/sec.

After some practice one can, without too much difficulty, cleave a large film which contains thin regions step-free on both sides. The uniform area should be at least 1 cm^2 in order to cut two rectangular pieces from it with hot platinum wire.

The newly cleaved film is placed across two clean metal blocks (Figure 3.4, d), and held by two smaller metal blocks over its edges. Platinum wire of diameter 0.2 mm is mounted between two parallel conducting rods and heated above the melting point of mica by passing a low voltage current through the platinum wire. By adjusting the current through the platinum wire, it becomes hot and firm sufficiently to cut the mica film without breaking the platinum wire. To be noted, it is very easy to break the platinum line while cutting thicker mica films. Gently move the hot platinum cutter to cut the mica film into rectangular shape. Hold the small piece with sharp tweezers at its edge, and attach it on the step free area of the back sheet. It should be very easy for two molecularly smooth mica surfaces attach and stick to each other while they are approaching each other. If it is not attaching, either the small sheet or the back sheet is contaminated, or the small sheet is too thick. Then another small sheet should be tried while discarding the poor one. Place each pair of the small sheets neighboring on the back sheet and draw a layout sketch accordingly on a notebook for later identification. Because mica is berefringent, the upper and lower mica surfaces in SFA experiment should have the same crystalline orientation. It is a good practice that one has a routine procedure, as shown in Figure 3.5, to make sure that surfaces has the "right" orientation.

(a) Trimming:
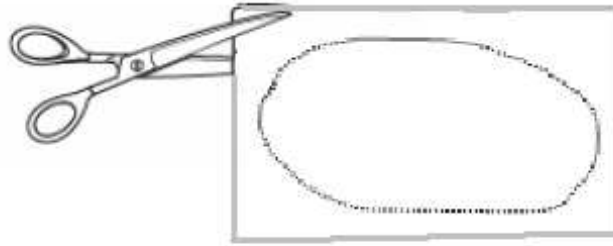
(b) Splitting:
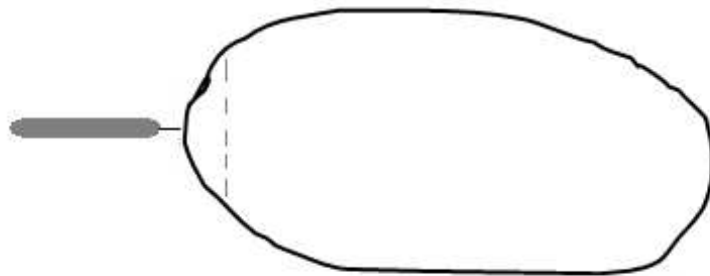
(c) Peeling:
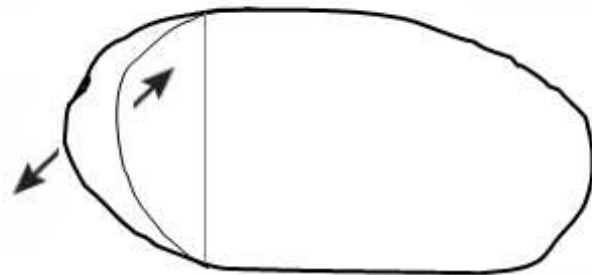
(d) Cutting:

+

-
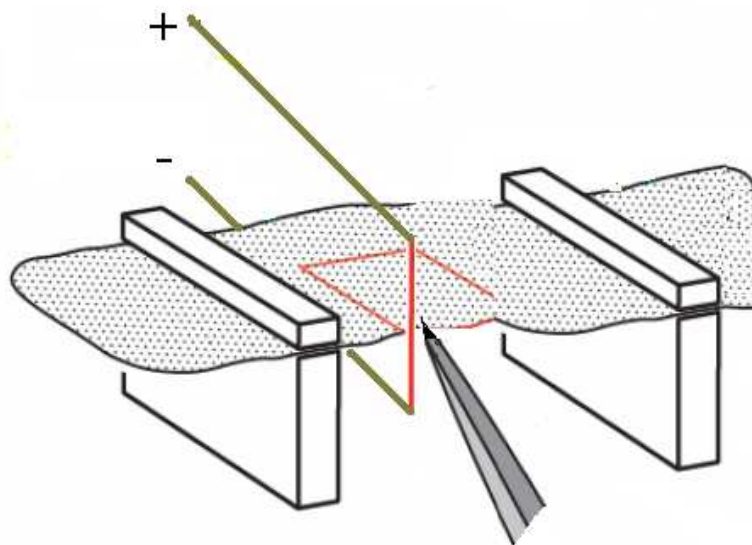
Figure 3.4: Procedures of peeling thick mica sheet into thin sheet containing step free region and cutting it into squares with hot Pt wire
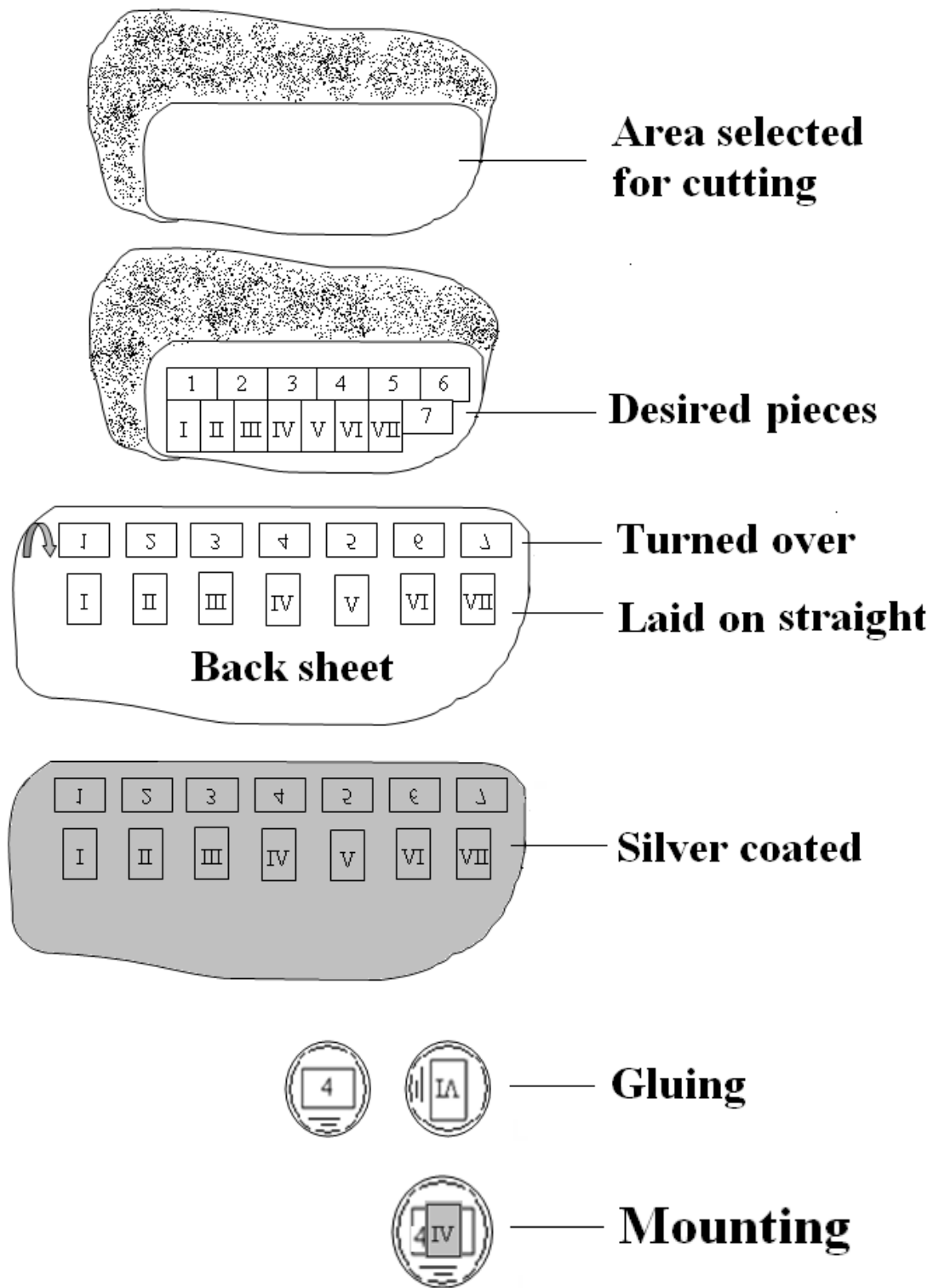
Figure 3.5: A suggested arrangement for mica sheets cutting, protecting, silvering, gluing and mounting in pairs:1 to I, 2 to II,…

3.2.2 Silver coating on mica sheets

When several pairs of mica sheet are attached onto the back sheet, it is ready to deposit silver on the uncovered surfaces (Figure 3.5). The silver deposition on the exposed mica sheet surfaces is achieved with a CVE 301 vacuum coating system. First put the backsheet with the small thin mica sheets facing down towards the silver shots. Create a high vacuum with a pressure below 5×10^{-6} torr before heating the silver shot. The silver

thickness deposited on the mica film is measured with a QCM sensor. To have the best performance in later optical multiple beam interference experiment, a thickness of 500 Å deposited at 1 Å/s is advised.

After silver coating, one should see a shining surface of silver on the back sheet. It is refrective but remains transparent. Let the system cool down for half an hour, and then remove the mica back sheet to the dust free laminar flow cabinet.

3.2.3 Gluing of mica to silica disk

Silica disks were purchased from Esco Products Inc., USA. The silica disks act as optical windows and support for mica films. Each disk is a round disk with two polished surfaces. The radius of the disk is about 10 mm, and the thickness is about 4 mm. One of the two surfaces is optical flat and the other is cylindrically curved, with a radius of about 20 mm. Different glues were used to glue mica films on silica disks. The choice of the glue depends on the medium type of force measurements. For aqueous solutions, crystals of EPON RESIN was used, but for organic solvent such toluene, sugars such as glucose, dextrose and galactose were good choices. After putting silica disks on a small

electrically heated hot plate, a tiny amount of glue in powder form (EPON RESIN or sugars) was placed on the top cylindrically curved surfaces of the disks. As the glue melted into liquid, curved tweezers were used to spread it evenly over the curved surfaces. The spreading direction was always on the axis direction of the cylinder surface. After spreading for several times, the final thickness of the uniform glue layer should be about 20 μm. The temperature was adjusted so that it would not over-heat the silver layer which was glued onto the disk. The over-heated silver layer would turn into opaque and white yellowish color which would reduce the reflection and hence the quality of FECO. performance. Over-heating of the glue could also trap some bubbles into glue layer, leading to poor quality of FECO.

While the glue layer was spread evenly on the curved surface of silica disks, a small mica sheet was peeled off from the back sheet with sharp tweezers and placed on the top of the glue layer by holding the small mica film with silver coating facing down. The longitudinal direction of the rectangular small mica film was arranged parallel with the axis of the cylindrical surfaces. It is important to make sure that the mica film was evenly attached onto the surface without any buckling or bubble inside. The disk was then removed from the hot plate. Bare mica surface was ready for experiment or further modifications.

3.2.4 Thin film preparation

If one would like to study mica-mica interactions in some media, mica films mounted on silica disks are ready for being mounted in SFA. However if one intends to measure

interactions between materials other than mica, coating of thin films on the prepared mica surface is required.

Thin film can be deposited onto the mica film with different methods such as Langmuir-Blodgett deposition, dipping or spin coating. The detail of the thin film preparation will be covered in later chapters.

3.2.5 Assembly of SFA

When surfaces are prepared on the silica disks, the disks should be mounted into the disk holders of SFA 2000. First the lower disk was placed into the disk holder connected to the force cantilever with mica film facing up. The disk was fixed on the disk holder by tightening the side screw. The direction of the axis of the cylindrical surface was arranged either normal or parallel to the front wall of the chamber. The cantilever was then lowered to make sure there was enough room for upper surface so that the two surfaces would not touch each other when assembling. The other silica disk was mounted in the disk holder on the piezo-mount with the mica surface facing out. Again the silica disk was fixed by tightening the side screw. The piezo tube with the mounted silica disk was inserted in such a way that the two mica surfaces were facing center to center with axis being perpendicular. The piezo tube was then tightened onto the main chamber of SFA, as shown in Figure 3.3. There may be two configurations according to the orientation of the disks. For normal force measurement these two configurations makes no difference as long as the two axes of cylindrical surfaces are strictly perpendicular to each other. The apparatus was then placed on a vibration-free table. The white light beam was guided to pass through the bottom window of the apparatus as described in Figure

3.6. Two surfaces were brought close by rotating the micrometers mentioned earlier in this chapter. The microscope tube was placed into piezoelectric tube, and a prism was placed on top of the micrometer to reflect the interference image into a spectrometer. .
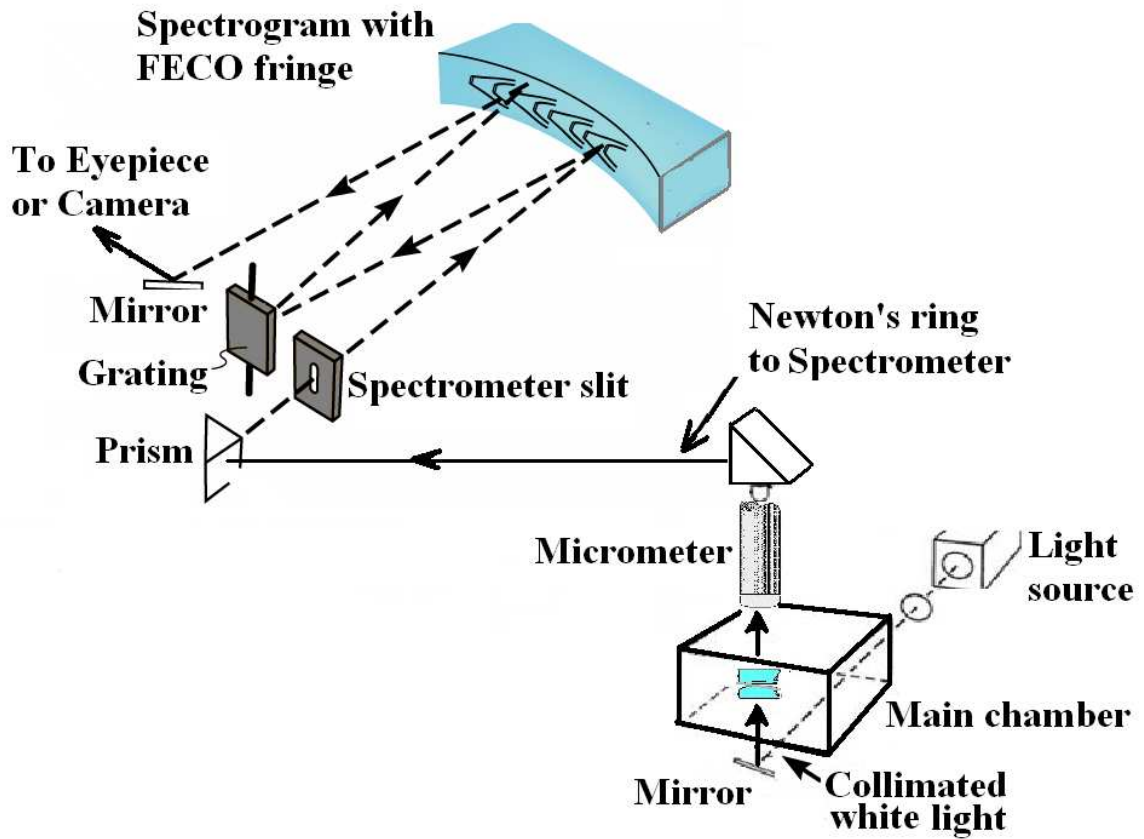
Figure 3.6: Surface force apparatus system

3.3 Multiple Beam Interferometry (MBI)

In SFA experiment, the absolute distance between two surfaces is measured by the multiple beam interferometry (MBI) method [Israechvili, 1973]. The measurement can be accurate down to 0.1 nm with very thin separations. In MBI method, the outer sides of a pair of transparent surfaces (such as mica) were coated by a highly reflective multidielectric layers (such as silver, aluminum), which acted as mirrors. In SFA experiment, as shown in Figure 3.7, a beam of white light came in consequently through layers of silica, silver, mica, media, mica, silver, silica, and finally to the spectrometer. The two silver layers acted as mirrors so that white light experienced multiple reflections and multiple interferences between the two reflecting silver layers. Only certain wave lengths from the white light passed through. If an eye piece, instead of a prism was put on top of the microscope, Newton's ring could be seen from the eye piece. With the prism, the Newton's ring was then guided into a spectrometer and the discrete wave lengths were split up and appeared as an array of fringes in the spectrogram. These fringes are called "Fringes of Equal Chromatic Order" (FECO), which had been studied extensively by Samuel Tolansky, a professor of physics at the London University [Tolansky, 1949]. FECO patterns contain a lot of information including the separation of the two surfaces, the topography of the surfaces, the refraction index of the media and the thickness of the mica films [Heuberger, 1997; Tadmor, 2003].
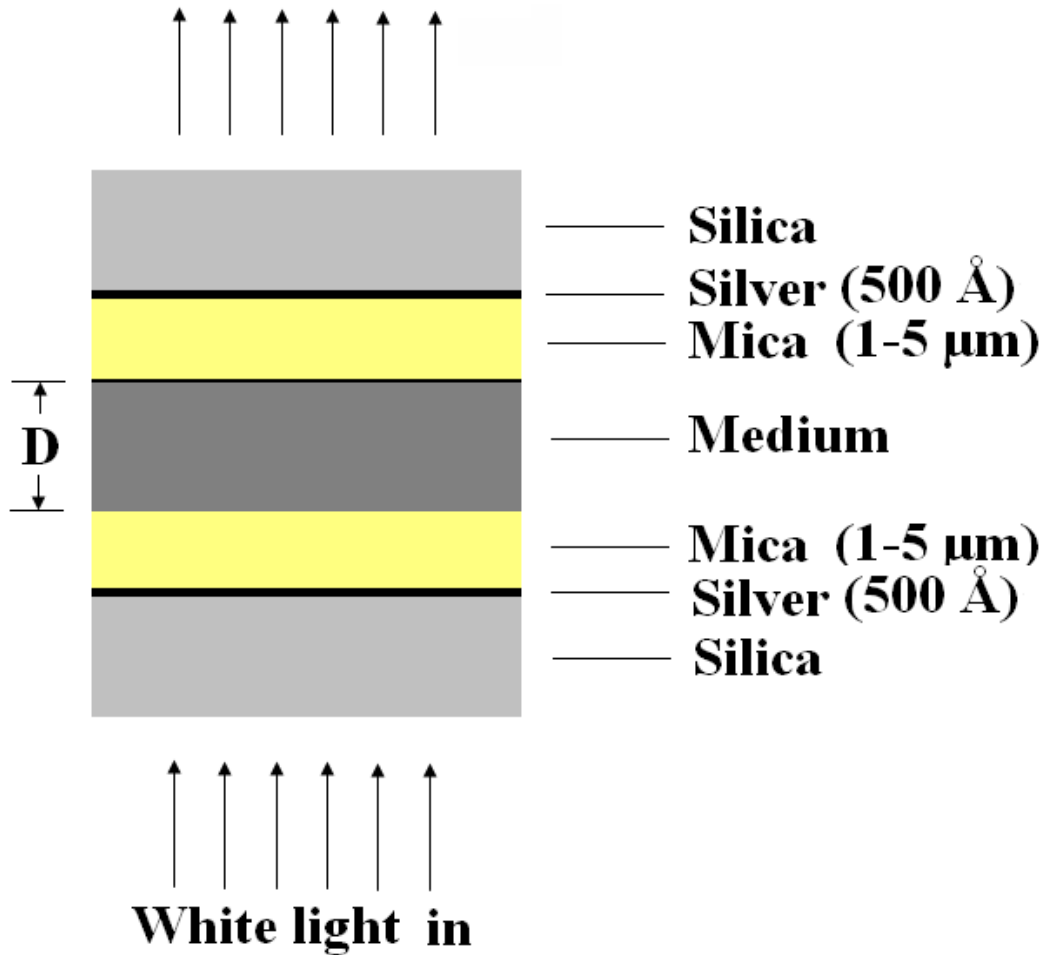
Figure 3.7**:** Multiple beam interferometry (MBI):
White light pass through layers of silica, silver, mica, medium, mica, silver,
silica,   and undergoes multiple reflections between two silver layers

3.4 Introduction of FECO Interferometry

When the two back silvered sheets of mica surfaces are in contact, the FECO patterns appear in the exit port of the spectrometer as an array of sharp colored fringes as shown in Figure 3.8A. The flat part in the fringes represents the flat topography of the contacted area. This is a unique characteristic of the MBI technique, and was widely used for surface topography analysis. The discrete FECO fringes represents discrete wavelengths λ_n^0 (n=1, 2, 3,...), where n is the order of the fringes after the MBI interference.

When the surfaces are separated apart by separation D, the flat surface area disappears and so does the flat part of the fringes. The fringes do not only change shapes but also shift to longer wavelengths λ_n^D (n=1, 2, 3,...) . Then a FECO pattern as shown in Figure 3.8 B will appear. If the two mica sheets have the same thickness, the relationship between λ_n^0 and λ_n^D is given by equation (3.1):

$$\tan(2\pi\mu D / \lambda_n^D) = \frac{2\overline{\mu}\sin\left[\dfrac{1-\lambda_n^0/\lambda_n^D}{1-\lambda_n^0/\lambda_{n-1}^0}\pi\right]}{(1+\overline{\mu}^2)\cos\left[\dfrac{1-\lambda_n^0/\lambda_n^D}{1-\lambda_n^0/\lambda_{n-1}^0}\pi\right]\pm(\overline{\mu}^2-1)} \qquad (3.1)$$

Where + refers to odd order fringes and − is for even order fringes. $\overline{\mu} = \mu_{mica}/\mu$, where μ_{mica} is the refractive index of mica at λ_n^D, and μ is the refractive index of the medium between the two mica surfaces at λ_n^D.
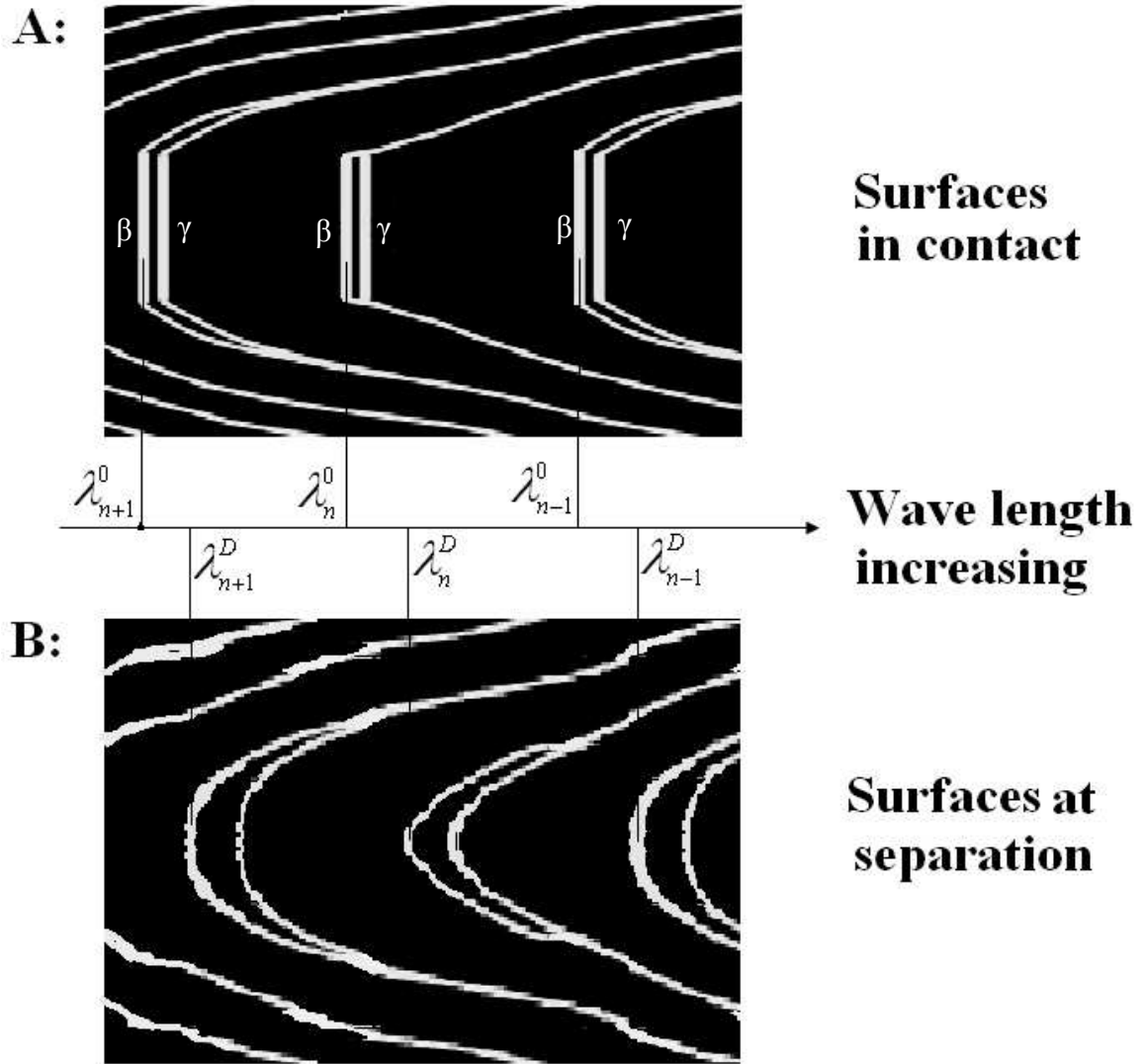
Figure 3.8: The shape of the fringes equal chromatic order (FECO) observed on the spectrogram of the spectrometer through the eyepiece or on a video monitor. The double β, γ fringes are caused by the birefringence of mica

For separations less than 30 nm, the above equation can be simplified to two approximation equations depending on odd or even numbers of n:

$$D = \frac{nF_n(\lambda_n^D - \lambda_n^0)}{2\mu_{mica}} \; , \qquad \text{(n as odd number)} \qquad (3.2)$$

$$D = \frac{nF_n(\lambda_n^D - \lambda_n^0)\mu_{mica}}{2\mu^2} \; , \qquad \text{(n as even number)} \qquad (3.3)$$

where
$$nF_n = \frac{\lambda_{n-1}^0}{\lambda_{n-1}^0 - \lambda_n^0} \qquad (3.4)$$

nF_n can be considered as a correction factor due to the phase changes at mica-silver interfaces and the dispersion effects (for measurements at $\lambda \sim 550$ nm $, nF_n \approx 1.024 + 1/n$).

The shift in wavelengths is different for the odd and the even fringes. For odd fringes, the shift is not dependent on the refractive index of the media, but only dependent on the separation and the refractive index of the mica.

By measuring the shifts in wavelengths of an odd and its neighboring even fringe, the equation 3.1 can be solved simultaneously for both distance D and the media refractive index μ. Below 200 nm separation the accuracy for the separation distance D is at the level of 0.1 nm.

The refractive index of mica μ_{mica} can be predetermined by Abbé refractometer. Since the mica is birefringent, it shows slightly different refractive index while measured with different orientations. For the FECO fringes, every fringe should appear doublet if two surfaces are placed with the same orientation. Otherwise the doublet fringe looks fat and blurring.

In this study, both wavelengths of the fringe doublet were always measured, and then the average of the two was taken for better accuracy in the analysis using equation (3.1).

3.5 Local Radius of Surfaces

As mentioned before, FECO technique had been used for surface topography studies [Tolansky, 1949; Heuberger, 1997]. For SFA force measurements, the surface curvature (local radius of surface) is needed to normalize the measured surface forces.
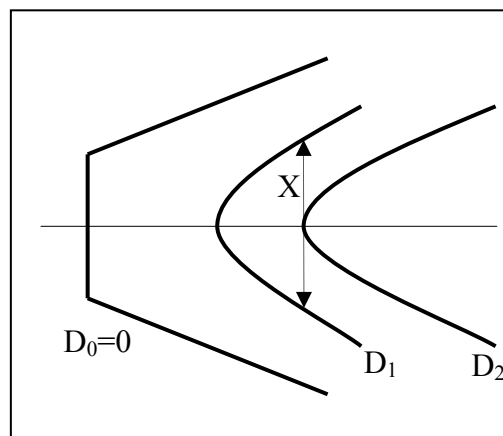
Figure 3.9: Measurement of surface curvature:
The nth fringe moves from left to right in the spectrogram

As shown in Figure 3.9, an individual FECO fringe of nth order was recorded in one frame, while the surfaces were set apart from contact to D_1 and bigger D_2. The nth fringe had moved from left to right. The fringe shape and wavelength were changed, as distance increased. D_1 and D_2 were measured by method metioned earlier with Equation (3.1). X is the distance on the eyepiece at the apex of D_2 fringe, f is the optical magnification factor from surface to eyepiece in vertical direction.

$$R_{\parallel} = \frac{(X/f)^2}{8(D_2 - D_1)} \tag{3.5}$$

By rotating the white light beam 90 degrees with a DOVE prism before it entered the SFA main chamber, an other set of local radius of the surface was obtained. These two perpendicular radii $R_{\perp}$ and $R_{\parallel}$ represented the surface curvatures of two perpendicular cylinders. Since the two radii are usually very close, a geometric average $R = \sqrt{R_{\parallel} R_{\perp}}$ is chosen as the radius to normalize the surface force.

CHAPTER 4 MEASUREMENT OF INTERACTIONS BETWEEN ASPHALTENE SURFACES IN TOLUENE AND HEPTANE BY SFA TECHNIQUE

4.1 Interactions of Asphaltene Surfaces in Organic Solvents

The heavy oil, also known as bitumen in Alberta oil sands contains 10% to 20% asphaltene by weight[Masliyah, 2007]. As it does to the conventional oil industry, asphaltene causes threats to oil sands industry as well [Mullins, 2007; Menon, 1986; Mclean, 1997; Zhang, 2003; Wang, 2009].

To extract bitumen from oil sands by the open pit mine method, oil sands are shoveled and trucked to extraction plants for separation. One million tons of ore and waste may be moved per day for smooth operation in a typical plant. After the gravitational separation and flotation extraction, the recovered bitumen froth typically consists of 60% bitumen, 30% water and 10% solids by weights. Solids and water need to be removed before sending the bitumen to the downstream upgrading facilities. The problem is that the extraction plants are built as close as possible to the mine, and the upgrading facilities are built far away from mine due to economy reasons. Normally pipelines from 40km to 500km length are used to transport the bitumen froth. The asphaltene in bitumen makes the handling and transport of bitumen challenging due to unexpected deposition and pipeline blocking [Mullins, 2007].

The bitumen froth can be diluted with naphtha to reduce the viscosity and density of organic phase for easier transport and handling [Masliyah 2007]. Coarse solids are removed by centrifugation at 250g and the fine solids and water droplets are removed by further centrifuge at 2500g. Due to the corrosive characteristic of salty water, upgrading operations are experiencing difficulties with bitumen feed containing 2-3% of salty water. The remaining 2-3% water is trapped in the form of stable water-in-oil (w/o) emulsions. Asphaltenes are believed to be the key factors in stabilizing w/o emulsions by their absorption at oil-water interface due to their amphiphilic characteristics [Yarranton, 1997].

Asphaltene is commonly defined as the molecular fraction in crude oil or bitumen that is soluble in toluene but insoluble in n-heptane. Basically asphaltenes are a mixture of complex organic compounds. Since it is more of a practical than theoretical definition, the composition of asphaltenes varies with different originations. The behavior of asphaltenes behavior is very sensitive to the environment[Mullins, 2007]. A small changing in solvent ratio, temperature and/or pressure may lead to asphaltene aggregation or precipitation in pipeline or processing vessel. It is therefore imperative to fully characterize the interaction forces between asphaltene surfaces in solvents to shed light on the stabilization mechanism of water-in-diluted bitumen emulsions and hence to develop strategies for effective removal of emulsified water droplets from diluted bitumen.

Significant efforts have been made during the past decades to understand the molecular characteristics of asphaltenes. Several microscopic and nanoscopic techniques, including

micropipette [Yeung, 2000], Langmuir trough[Zhang, 2007] and atomic force microscope (AFM)[Liu, 2004], have been applied to characterize the surface interactions of asphaltenes in the context of w/o emulsion stabilization mechanisms. The micropipette technique was used to study the interface of water-diluted bitumen by measuring the interfacial properties such as interfacial tension of micrometer-size emulsion droplets. Langmuir trough was used to measure the surface pressure of the asphaltene layers formed at the water and toluene interface. The Langmuir trough results showed that asphaltene layers are rigid and hard to wash away by the addition of fresh toluene. This is why it is difficult to disrupt the protective asphaltene layer surrounding the emulsified water droplets in diluted bitumen. Very recently, AFM was applied to direct measurement of the interaction forces between asphaltene films against a microscopic silica sphere in both aqueous and oil media. The above research provided valuable information on the steric origin of repulsive force and stabilization mechanism of the water-in-diluted bitumen interface. Yet, due to the complexity of the problem and certain limitation of the techniques used, a full fundamental understanding of surface properties, intermolecular and surface interactions of asphaltenes, and the governing mechanisms of stabilizing water-in-oil emulsions remains incomplete. Developing full understanding of intermolecular forces would be of great value in many engineering processes of bitumen and crude oil production.

In addition to the Naphtha treatment used by the pioneer operations, paraffin treatment was successfully batch tested by Syncrude, CANMET and CONRAD[Shelfantook]. Naphtha is a good solvent for bitumen while paraffin diluent is a poor solvent such as

pure heptane or hexane. Above a given diluent to bitumen ratio, paraffin solvent can precipitate the problematic asphaltenes with solids and water droplets being trapped inside. As a result, diluted bitumen can be solid and water free. This novel approach had been commercially used by Shell Albian Sands and attracted great interests to new mine operations [Masliyah 2007].

The composition of paraphin has a huge effect on the asphaltene precipitation. The industry is demanding a better understanding of the surface forces between asphaltenes in organic solvents. Some pioneer research on this field has been carried out with AFM colloidal force technique [Wang, 2009; Wang, 2010]. The surface forces apparatus (SFA) technique is a complementary technique for such research objectives, which has been used extensively in many other areas of research, both biological and non-biological, due to its unique ability to provide both direct measurement of forces, F, as a function of the absolute surface separation, D, and the local geometry of two interacting surfaces (the local radius R or contact area A) with a force sensitivity of ~10 nN and an absolute distance resolution of 0.1 nm measured in situ and in real time [Lin, 2005; Zeng, 2007]. Vuillaume et. al.[2009] applied the SFA technique to measure the interactions between mica surfaces in crude oil from Campos Basin, Brasil and asphaltene solutions.

In the present study, a surface force apparatus (SFA) was used to study the interactions of asphaltene surfaces in toluene and heptane and the adsorption mechanisms of asphaltenes to clay (mica) surfaces. The force vs. distance curves, or so-called force profiles, could provide valuable information on local material properties such as interaction energies,

Hamaker constant, and molecular conformation changes of the interacting asphaltene surfaces or films. Atomic force microscopy (AFM) was used to provide complementary information on the surface morphology of asphaltene films studied.

4.2 Experimental

4.2.1 Materials

Vacuum distillation feed bitumen was provided by Syncrude Canada Ltd. Toluene (Optimal) was purchased from Fisher Scientific and n-heptane (HPLC) was obtained from Sigma–Aldrich. Mica is purchased from S&J trading (Glen Oaks, NY).

4.2.2 Asphaltene preparation

Asphaltene was obtained by solvents precipitation from bitumen[Zhang 2003]. The bitumen was first diluted in toluene at a volume ratio of 1:5. The fine solids in bitumen were removed by centrifugation of the diluted bitumen at 20,000 rpm for 30 min. The toluene was then removed from the bitumen solution by days of natural evaporation. Heptane was mixed with the prepared dry bitumen at a volume ratio of 40:1 to extract the asphaltenes. The n-heptane and bitumen mixture was shaken for 2 h in a bottle and left overnight for asphaltene precipitation. The supernatant was then decanted from the asphaltene precipitates. The asphaltene precipitates were repeatedly washed with n-heptane until the supernatant became colorless. The dry asphaltenes were obtained by

naturally evaporating the heptane solvent. The mass of the whole asphaltenes obtained as such was about 12% of the original bitumen.

4.2.3 Asphaltene surface preparation

Asphaltene films were prepared by dip coating method. Asphaltene toluene solution was prepared to 0.5wt%. The solution was filtered with a WHATMAN 0.2um PTFE filter before the dip coating.

Fresh mica surface was prepared as described in Chapter **3** using glucose as glue. After the newly prepared mica was mounted on a silica disk, the whole disk was dipped into 0.5wt% asphaltene solutions for 5 minutes. The surface was then thoroughly rinsed with toluene for at least 10 times to ensure that the back surface of the silica is clean and clear. The new asphaltene thin film was let dry by placing the silica in a laminar hood for half an hour.

4.2.4 AFM characterization of asphaltene films

The newly cleaved mica surface and asphaltene coated mica surfaces are characterized by AFM. The taping mode surface image was obtained in air with a Nanoscope E AFM (Digital Instrument, Santa Barbara, CA, USA).

4.2.5 Force measurement

A surface forces apparatus, SFA 2000 (Surforce LLC, Santa Barbara, CA, USA) [Israelachvili, 1973, 1992] was used to determine the normal interaction forces between

two asphaltene surfaces in organic solvents or two curved molecularly smooth surfaces of mica across (immersed in) toluene or heptane containing various concentrations of asphaltenes. Detailed setup for SFA experiments has been introduced in Chapter 3. Briefly, a thin mica sheet of 1-5 μm thick was glued onto a cylindrical silica disk (radius R=2 cm). The back surfaces of the mica sheet were coated with a ~50 nm thick, semi reflective layer of silver, required to obtain multiple-beam interference fringes of equal chromatic order (FECO. The FECO was used to determine the surface separation, surface shape, deformation and the contact area in real time and *in situ*. The two curved and coated mica surfaces were then mounted into the SFA chamber in a crossed-cylinder geometry, which roughly corresponds to a sphere of radius R approaching a flat surface. Based on the Derjaguin approximation, $F(D) = -2\pi RW(D)$, where $F(D)$ is the force between the two curved surfaces and $W(D)$, the interaction energy per unit area between two flat surfaces. For the SFA experiments, ~50 μL of the appropriate solvent/solution was injected between two closely apposed mica surfaces. The SFA chamber was sealed and saturated with the same solvent. The reference distance ($D = 0$) was set as the adhesive contact between the two bare mica surfaces in air prior to putting the solvents between the surfaces. Normal forces between the two surfaces were measured by moving the lower surface supported by a double-cantilever 'force springs' by a distance $\Delta D_{applied}$. The actual distance that the surfaces moved relative to each other, ΔD_{meas}, was measured by multiple beam interferometry. The change of force ΔF between the surfaces, when they came to rest at a separation D, is therefore, $\Delta F(D) = k (\Delta D_{applied} - \Delta D_{meas})$, where k is the spring constant. When $\partial F(D)/\partial D > k$, there is a mechanical instability and the lower

surface will jump either toward or away from the upper surface during approach or retraction, respectively.

Surface force measurement was performed in a good solvent of toluene, and a poor solvent of n-heptane. Three sets of surface configurations as shown in Figure 4.1 were used in the SFA force measurement.
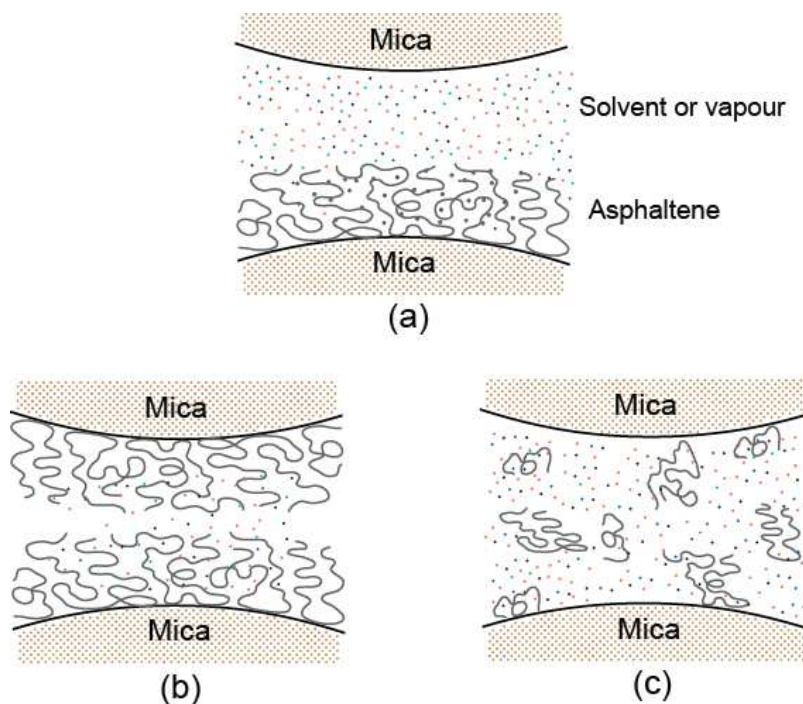

Figure 4.1 (a) Asymmetric coating, (b) Symmetric coating, and
(c) Asphaltene solution between mica surfaces.

Figure 4.1a shows an asymmetric geometry of an asphaltene film on one mica surface interacting with a bare mica in the solvent of interest. Figure 4.1b is a symmetric geometry in which both mica surfaces are coated with an asphaltene layer interacting in a

solvent. Figure 4.1c shows the bare mica surfaces interacting in a toluene solution of various asphaltene concentrations.

For each force measurement, it is important to have the wavelength reference with bare mica – mica surfaces in contact, and mercury characteristic lines on the recorded FECO images. For force measurement involving the coated asphaltene layers, the dip coating procedure should be after recording the reference fringes of bare mica-mica in contact.

Every force measurement includes an approaching force run and a separating force run. First, two surfaces were brought to several hundred nanometers apart by different stages of micrometers. The fringe images were recorded while the bottom surface cantilever was driven towards up surface at a constant speed. The two surfaces approached each other from zero force range, interacted in the force range and finally stopped at the hard wall. After it reached the hard wall, the fringes would not move anymore. Before separating force run, the motor was stopped to compress the two surfaces for a given period from 10 minutes to 1 hour. Separating force run was carried out by reversing the voltage applied to the cantilever motor. The separating speed is close to but not necessarily the same as the approaching speed even with the same applied voltages on the motors due to mechanical issues.

4.3 Results and Discussions

4.3.1 AFM images

Figure 4.2a is the AFM topography image of freshly cleaved mica surface. The fresh mica shows a featureless flat surface.

Figure 4.2b shows the AFM image of the dip coated asphaltene film on mica surface. In contrast to the bare mica surfaces of Figure 4.2a, the asphaltenes deposited on the mica surfaces are in the form of aggregates, several nanometers by width and several microns by length. It is much rougher than the bare mica surface. It is clear that the asphaltene is successfully deposited onto the mica surface. This dip coated asphaltene film from asphaltene in toluene solution has a similar morphology of the single layer of LB coating at higher surface pressure from air-water interface [Zhang 2003].

Two dip coated asphaltene samples were dipped into toluene and heptane for 30 minutes. The samples were then taken out and dried in air prior to the AFM imaging (Figure 4.5).
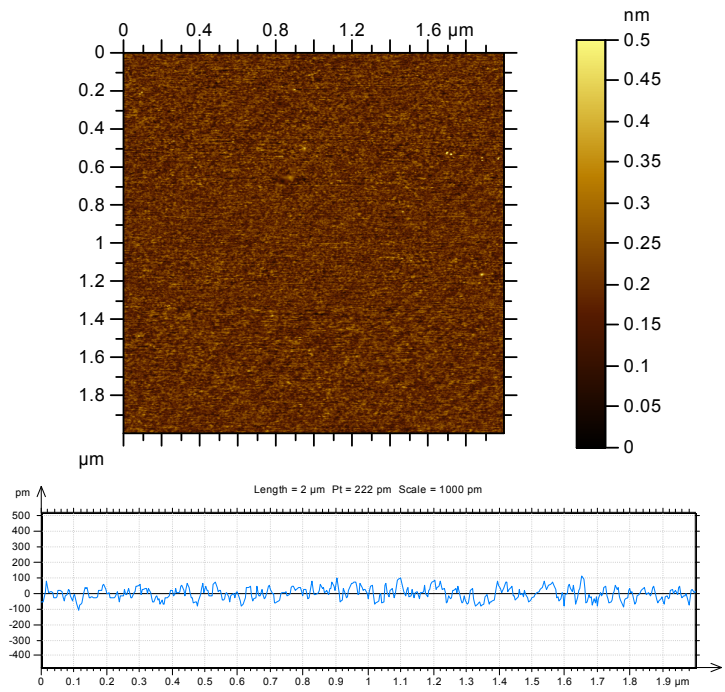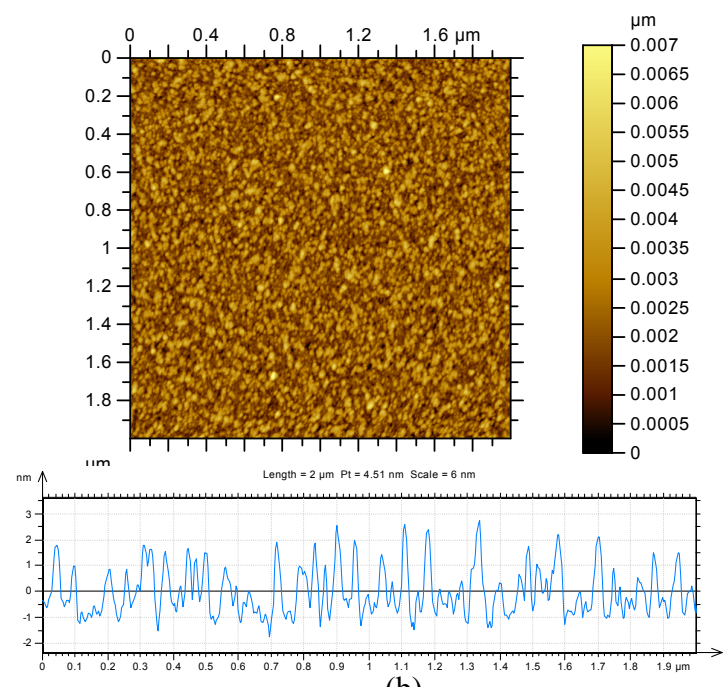
Figure 4.2 (a) AFM image of fresh mica surface;
(b) AFM image of dip coated asphaltene film on mica surface

4.3.2 Interaction forces of mica – mica in toluene:

Asphaltenes are soluble in toluene. Hence, toluene can significantly mediate the configuration of asphaltene molecules on a substrate, affecting the interaction forces. For this purpose, the force profile of mica surfaces in dry toluene was first determined. As shown in Figure 4.3, an attractive interaction force was measured as the two mica surfaces approach each other. The two surfaces jumped at D_J~7.5 nm into contact due to the van der Waals attraction between the mica surfaces across toluene. When the surfaces were separated, the surfaces jumped apart from contact showing a very strong adhesive force. For two surfaces 1 and 2 in a geometry of two crossed cylinders having the same radius R approaching each other in a medium 3, the attractive van der Waals force is given by Eq 4.1, and the critical jump-in distance D_J is given by Eq 4.2,

$$F_{vdW} = -\frac{A_{132}R}{6D^2} \tag{4.1}$$

$$D_J = \left(\frac{A_{132}R}{3k}\right)^{1/3} \tag{4.2}$$

where D is the distance between the two curved surfaces, k is the force-measuring spring constant, and A_{132} is the Hamaker constant of the two surfaces 1 and 2 interacting across 3. A_{132} can be estimated using Eq 4.3,

$$A_{132} \approx (\sqrt{A_1} - \sqrt{A_3})(\sqrt{A_2} - \sqrt{A_3}) \tag{4.3}$$

where A_1, A_2, A_3 are the Hamaker constants of media 1, 2, and 3 in vacuum. In our experiments, two surfaces of the same mica (medium 1 = medium 2) approach each other in toluene (medium 3). For the results shown in Figure 4.3, $D_J \approx 7.5$ nm, $k \approx 500$ N/m.

The Hamaker constant is $A_{mica-toluene-mica} = 3KD_J{}^3 / R \approx 3.2 \times 10^{-20}$ J from the experimental

estimation. The literature Hamaker constant values are $A_{mica} \approx (15.8 \pm 2.5) \times 10^{-20}$ J,

$A_{toluene} \approx 5.4 \times 10^{-20}$ J , Eq 4.3 gives $A_{mica-toluene-mica} \approx (\sqrt{A_{mica}} - \sqrt{A_{toluene}})^2 \approx 2.7 \times 10^{-20}$ J ,
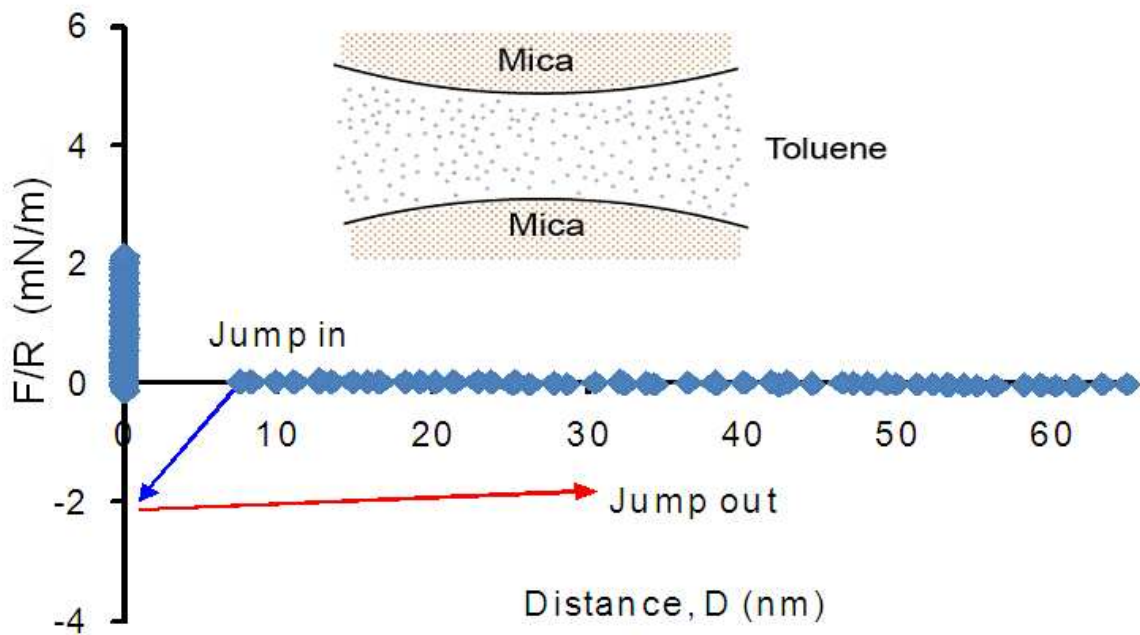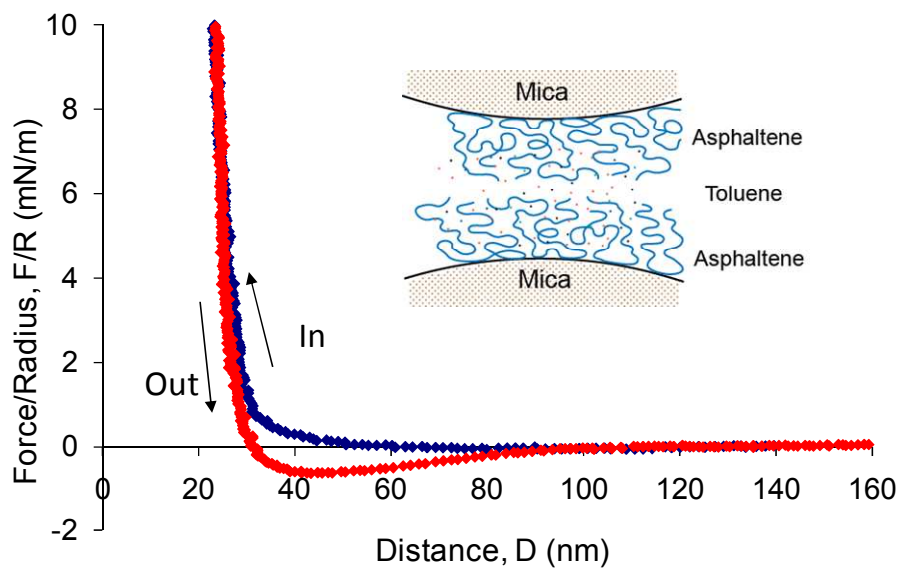
which is close to the above experimentally measured value.
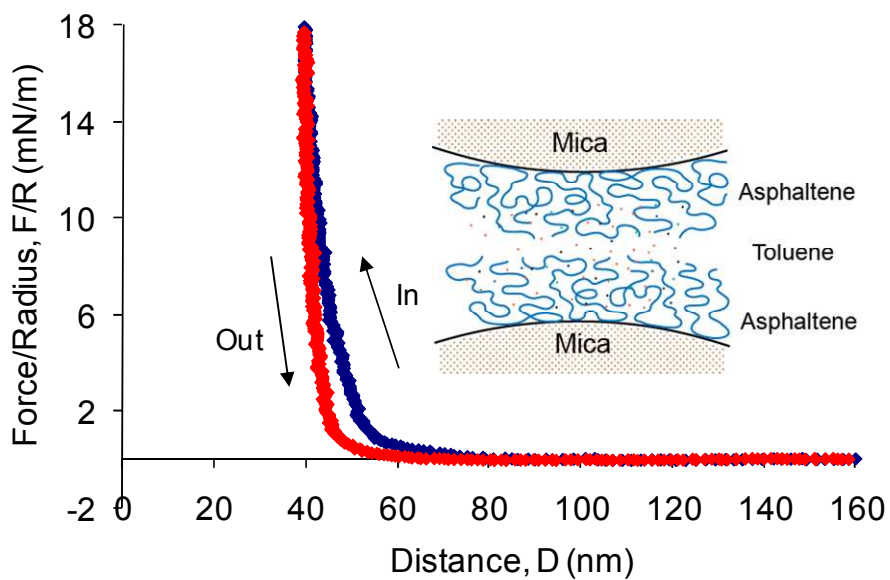

Figure 4.3 Mica – mica in toluene

4.3.3 Interaction forces of asphaltene- asphaltene in toluene

The surface force of symmetric asphaltene – asphaltene surface is ploted in Figure 4.4a. During approaching force run, only repulsive force is observed. At contact, the total thickness of the two asphaltene films is about 22 nm. Assuming both surfaces having the same thickness, the dip coated layer for one surface is about 11nm, which is about half of the thickness of the asphaltene coating in asymmetric force experiment as shown later. A weak adhesion force from about 30 nm was observed while separating the two surfaces from contact. Asphaltene film was dip coated on the mica surface. The orientation of asphaltene molecules should be therefore random. The polar groups and non polar groups can stick out from the surface at any direction. When the two surfaces are brought into contact under a sufficient external force, adhesion force is developed by interdigitation of those groups.

After the first set of force run, the two surfaces were separated from each other for 30 minutes before another set of force run. Figure 4.4b shows the significant change between the first and the second force profiles. Two remarkable changes were: i) the hard wall thickness has swollen or expanded to 40 nm, which is about double the original thickness in the first force run; ii) the adhesion force is not observed during the separation force run. Toluene is a good solvent for asphaltene. It can make the brush like asphaltene branches [Long 2007] stretch out in the solvent. It can also conformationally rearrange and form aggregates. This morphology difference was observed by the AFM images of dip-coated asphaltene surfaces before and after being immersed in toluene for 30 min, as shown in Figures 4.5a and 4.5b.

Figure 4.4 (a) The first force run of asphaltene – asphaltene in toluene
(b) The second force run of asphaltene – asphaltene in toluene
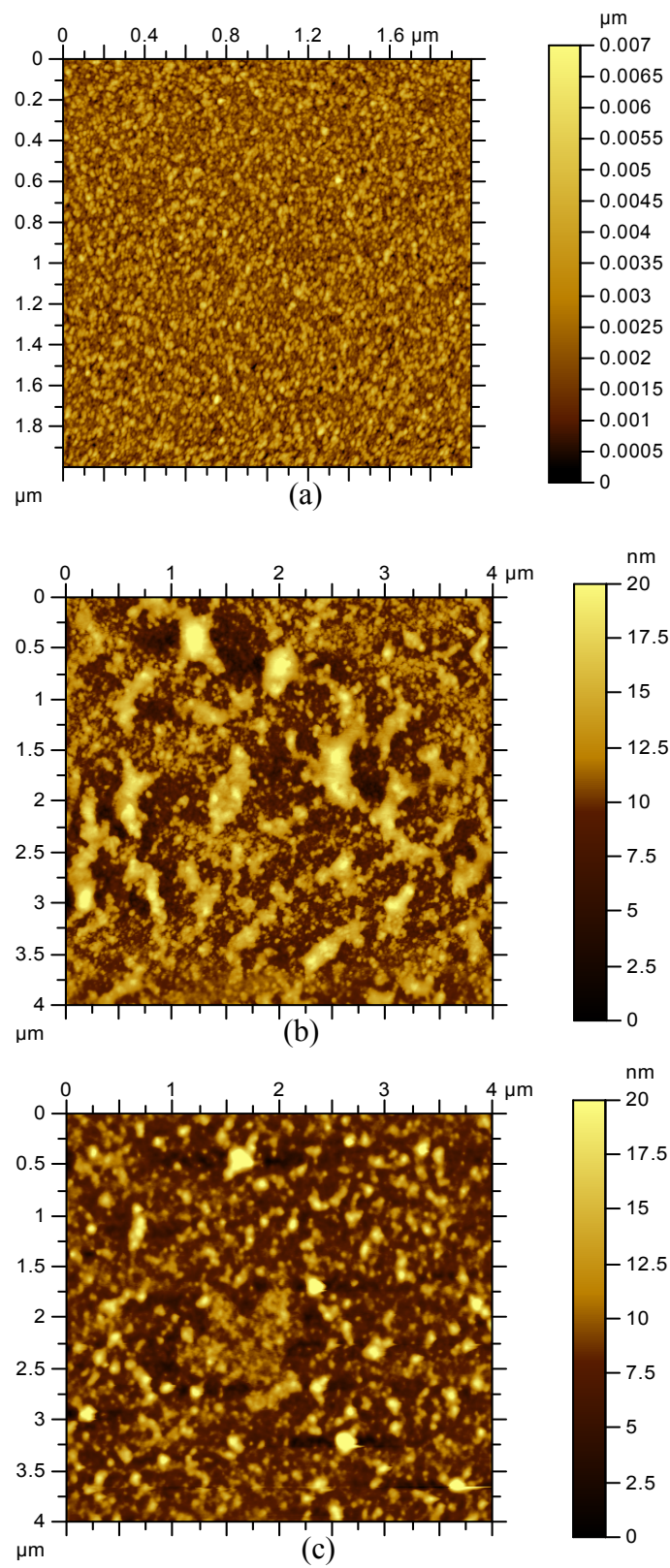30 minutes after the first force run

Figure 4.5 AFM images of (a) Dip coated asphaltene film on mica substrate; (b) Asphaltene coated surface dipped in toluene for 30 min; (c) Asphaltene coated surface dipped in heptane for 30 min.

While the two surfaces are brought back again, the extruding branches repel each other due to steric restriction. This hypothesis explains why the thickness of hard wall expanded and the adhesion force disappeared during the separation force run.

If we compress the two surfaces hard enough (~1 MPa) by using the manual micrometer, the hardwall can finally shift to ~11 nm. That is about the thickness of two monolayers[Zhang, Wang 2009]. This finding suggests that dip coated asphaltene layer can be compressed to monolayer.

4.3.4 Interaction forces of Asphaltene-mica in toluene

The interactions between dip-coated asphaltene surface and bare mica were also measured in toluene. Figure 4.6a shows the interaction force measured after the asphaltene exposed to toluene for ~ 1 hour. The two surfaces were brought into contact and then separated immediately. The repulsion during approaching starts at around 40nm with a hard wall distance ~ 22 nm. A weak adhesion force (F/R~-0.6 mN/m) was observed during separation. On successive approaching at the same position, asphaltene surface and mica were kept in contact for ~10 min. A much stronger adhesion F/R~-14.5 mN/m was measured as shown in Figure 4.6b. The repulsion starts at about 5 nm closer than the previous approaching in Figure 4.6a, while the hard wall shifts to ~18 nm. Under higher compression (~2 MPa) the hard wall shifts to ~5 nm, which corresponds to the thickness of one layer of asphaltene.

This experiment also shows that alphaltene can easily adhere to mica surface with contact or compression. The attractive van der waals forces may play a role in this process. If the applied separating force is less than 14.5mN/m, the adhered asphaltene layer won't come off from the mica surface. Cleaved mica has a silicate tetrahedron surface structure similar to some clay surfaces. Asphaltene from the bitumen can easily attach to clay fine particle, covering the surface and hence changing the surface wettability because of the amphiphilic characteristics of asphaltene. Finally the separation between bitumen and fine solids becomes very difficult resulting in a low bitumen recovery rate. This is why the clay contamination of oil sand ore is detrimental to oil sand bitumen extraction.
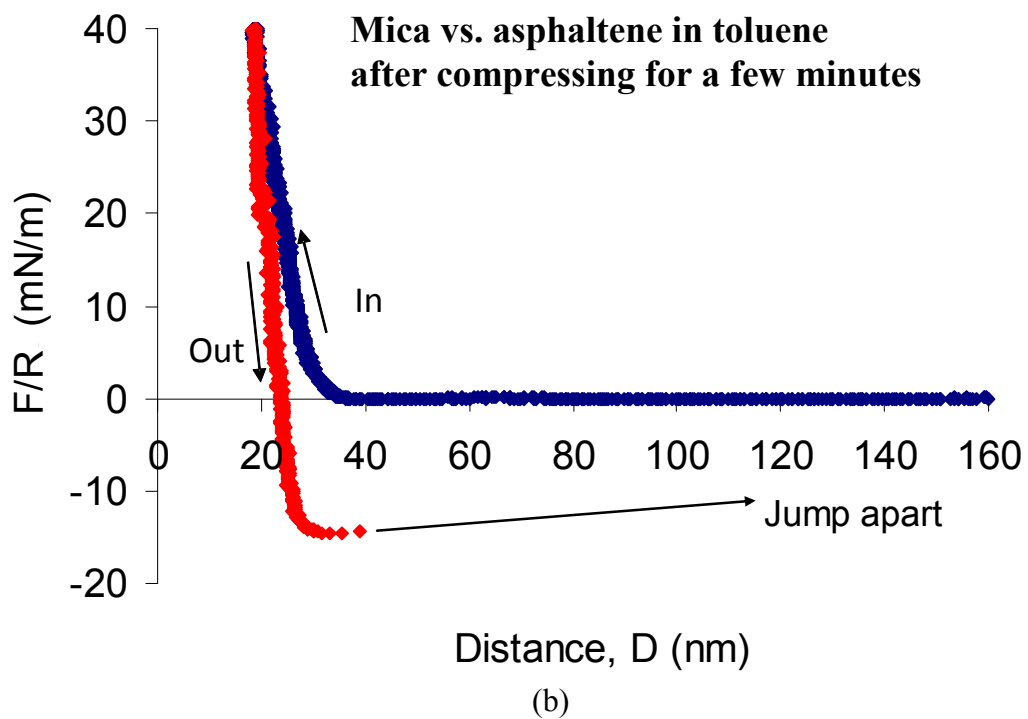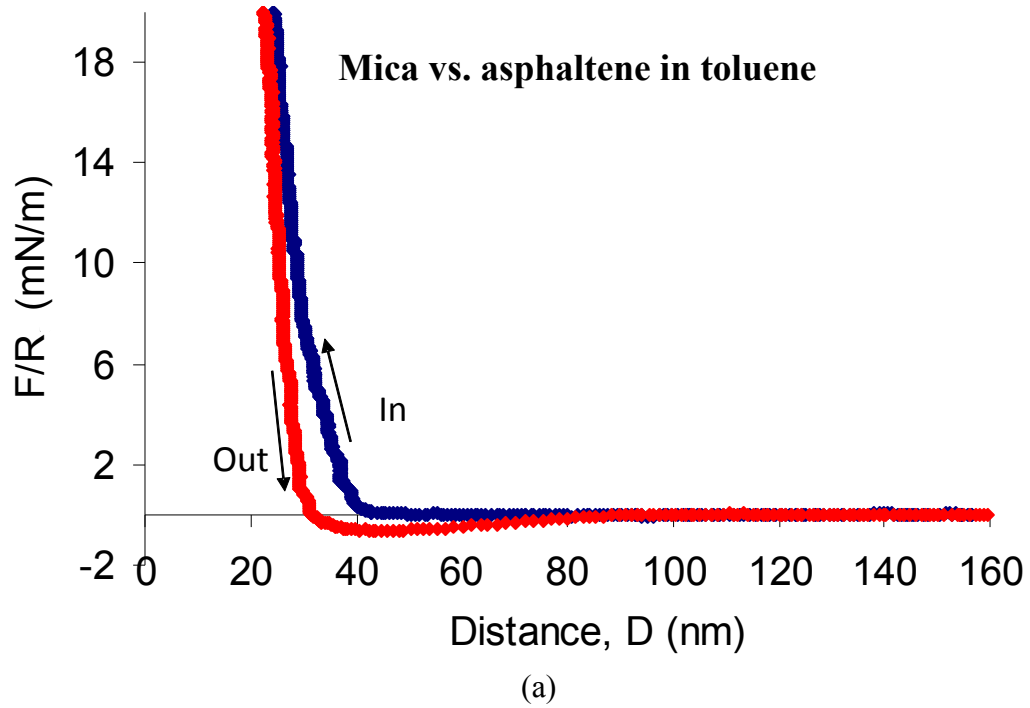
Figure 4.6 (a) Mica – asphaltene in toluene ;
(b) Mica – asphaltene in toluene after compressing for a few minutes

As toluene is a good solvent for asphaltenes, the tails or loops of the immobilized asphaltene molecules on mica surface tend to stretch and act as a swollen brush. Therefore, the coated asphaltene layer on mica may be treated as a polymer brush, and the interaction between two such layers could be described by the scaling theory for two interacting polymer brush layers [De Gennes, 1987]. When two polymer brush surfaces approach each other, at some distance the brushes start to overlap. The increased local density of polymer segments because of the overlapping leads to an increase in osmotic pressure and repulsive interaction energy. The repulsive pressure between two planar brush layers is given by

$$P(D) \approx \frac{kT}{s^3}\left[(\frac{2L}{D})^{9/4} - (\frac{D}{2L})^{3/4}\right] \text{ for } D<2L, \tag{4.4}$$

where s is the mean distance between anchoring (or grafting) sites on each surface, L is the brush layer thickness per surface, T is the temperature and k is the Boltzmann constant. For the geometry of two crossed cylinders of radius R (used in our SFA measurements), the force between them is given by first integrating the above equation and then using the Derjaguin approximation:

$$\frac{F(D)}{R} = 2\pi \int P(D)dD = \frac{16\pi kTL}{35s^3}\left[7(\frac{2L}{D})^{5/4} + 5(\frac{D}{2L})^{7/4} - 12\right]. \tag{4.5}$$

For the asymmetric case (a brush layer against a solid substrate), the equation becomes

$$\frac{F(D)}{R} = \frac{8\pi kTL}{35s^3}\left[7(\frac{L}{D})^{5/4} + 5(\frac{D}{L})^{7/4} - 12\right]. \tag{4.6}$$
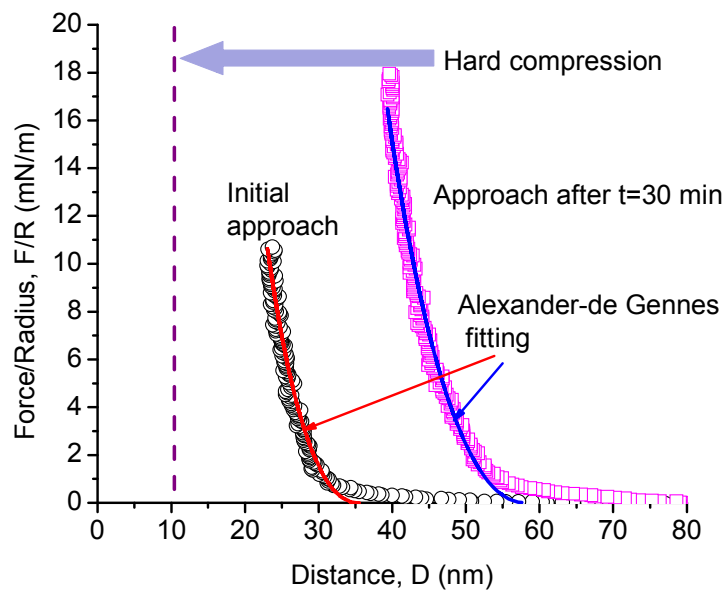
The measured repulsive forces and well fitted curves to the scaling theory (Eqs 4.5 and 4.6, solid curves) are shown in Figure 4.7, for approach of two asphaltene layers (Figure 4.7a) and an asphaltene layer against a mica surfaces in toluene (Figure 4.7b). The fitted

values of parameters *s* and *L* are listed in Table 1. The best fitted values of physical parameters in Table 1 indicate that the fitted mean distance between anchoring (or grafting) sites *s* on mica surfaces are very close to each other in two cases. The s values are close to size of so-called nano-aggregates of asphaltene in bulk toluene solutions. While the brush layer thickness *L* depends on compression pressure and immersion time in toluene, reflecting self-aggregation of asphaltene molecules. This findings is consistent with the surface morphology visualized using AFM, as shown in Figure 4.5.

Table 4.1. Fitting Parameters of the measured force profiles to
the Alexander-de Gennes Scaling Theory

Asphaltene surface vs. asphaltene surface		
Time after asphaltenes immersed in toluene (min)	~5	~35
L, nm	17.6	29.0
s, nm	2.8	2.7
Asphaltene surface vs. mica surface		
Time after asphaltenes immersed in toluene (min)	~60	~70[§]
L, nm	44.0	37.0[§]
s, nm	3.2	2.5[§]

[§]Under compression (~0. 5 MPa) before separation

(a)
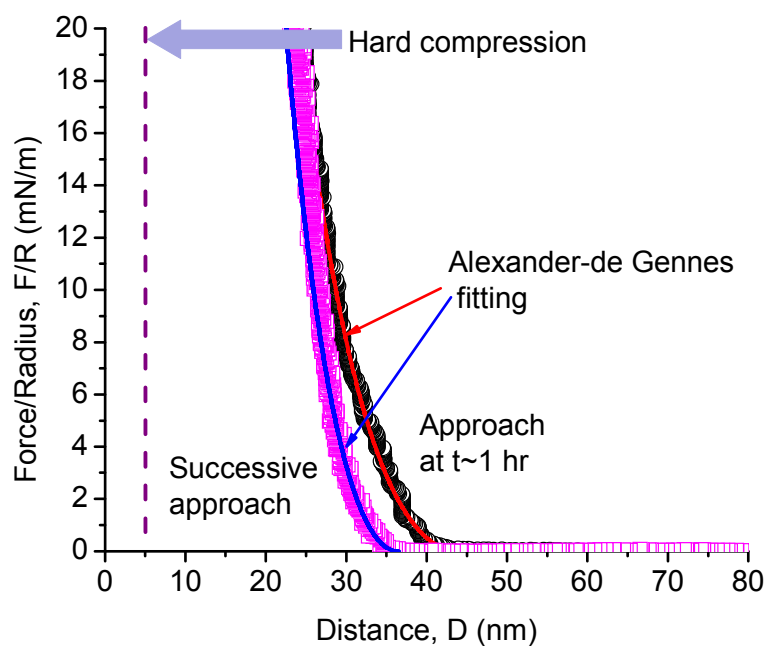
(b)

Figure 4.7 Experimentally measured repulsive forces and well fitted curves using the Alexander-de Gennes theory for approach of
(a) two asphaltene layers in toluene
(b) an asphaltene layer towords a bare mica surface in toluene.

## 4.3.5 Interaction Asphaltene - Asphaltene in Heptane (Poor solvent)

Heptane is aliphatic and apolar, while asphaltene molecules are highly aromatic with heteroatoms. Thus asphaltenes and heptane are very different in their molecular structures. It is well-known that heptane is a poor solvent for asphaltenes. Asphaltenes tend to self-aggregate and precipitate in heptane, which is very different from the case in toluene. The interaction force profile between two asphaltene surfaces in heptane is shown in Figure 4.8. The effective Hamaker constant of two aphaltene surfaces in heptanes is $A_{asphaltene-heptane-asphaltene} \approx 1.1 \times 10^{-21}$ J. The spring stiffness used for this experiment is $k \approx 880$ N/m. Eq. 4.2 predicts a jump-in distance $D_J = \left(A_{asphaltene-heptane-asphaltene} R / 3k \right)^{1/3} \approx 2$ nm for two smooth surfaces. However, no adhesive jump-in was observed during the approach of the two asphaltene surfaces, which was mainly due to the self-associate of the asphaltene molecules, resulting in rough surfaces. Strong adhesion force of $F/R \sim$ -3 mN/m was measured during the separation, as shown in Figure 4. 8a. The force profile indicates that asphaltenes were stretched for ~10 nm before the two surfaces jumped apart. Similar force profile was measured after 30 min as shown in Figure 4.8b. There is a weaker adhesion of F/R~ -1 mN/m and a slightly larger hard wall distance ~20.5 nm, as compared to ~16.5 nm of asphaltene films in toluene shown in Figure 4.8a.

The adhesion forces measured between two asphaltene surfaces in heptane are due to the van der Waals interaction, which demonstrates that van der Waals force is the dominant force leading to asphaltene flocculation in paraffinic solvents. Comparing Figure 4.4 and

Figure 4.8, one can observe clearly that the hard wall shift out more for two asphaltene surfaces in toluene (Figure 4.4a) than in heptane after 30min. The hard wall distance in the heptane system is ~20 nm shorter. The above results directly indicate that heptane is less favorable for asphaltene molecules to swell. For the heptane system, the hard wall distance was observed to shift out by ~4 nm after a 30-min incubation, as shown in Figure 4.8. This expansion of dip coated asphaltene agrees with observed morphology change of the asphaltene layers (swelling or molecular rearrangement).

From the AFM images in Figure 4.5b and 4.5c, we can see that asphaltene aggregate and swell in both toluene and heptane solvent, although the swelling is more significant in toluene. The morphological features of AFM images correlate well with the results of surface force measurement in Figure 4.4 and Figure 4.8. As asphaltenes are a complex mixture of so many compounds, both SFA force measurement and AFM imaging suggest that certain components of asphaltenes are able to have limited swelling in heptane, resulting in rearrangement and aggregation of asphaltene molecules to minimize the total energy in the heptane system.

The interactions between an asphaltene surface and a bare mica surface were also studied, and adhesion and interaction force profiles were similar in the toluene system.
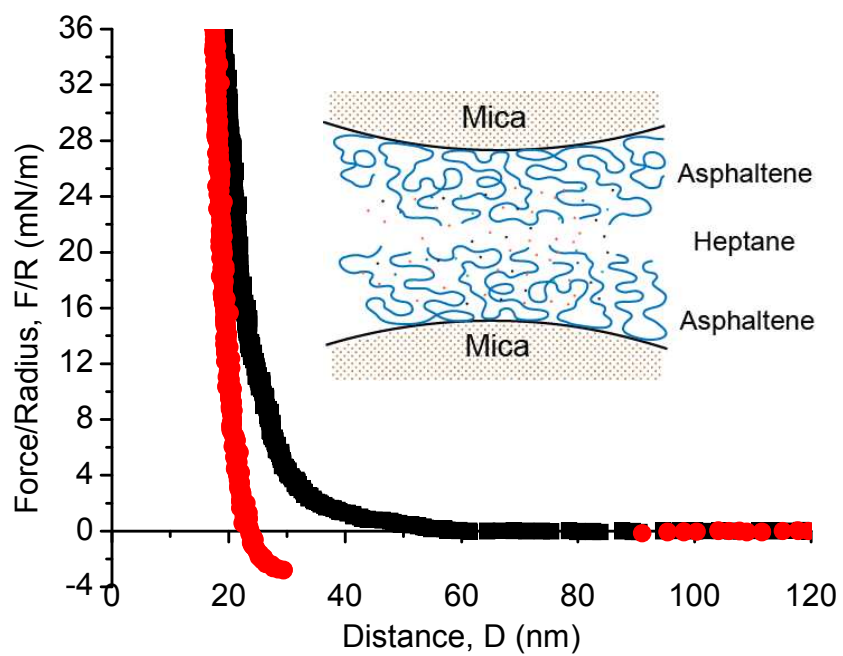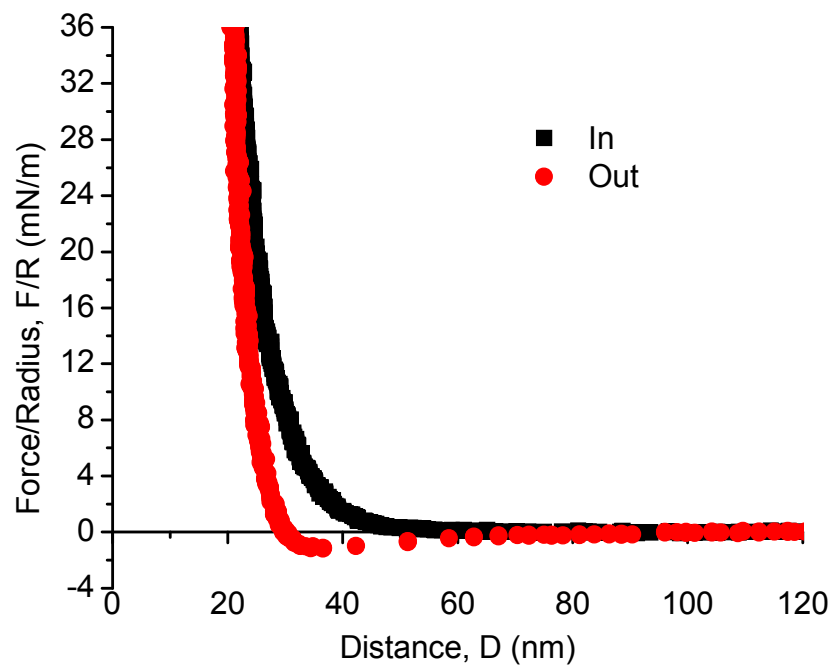
Figure 4.8 Surface force profile between asphaltene surfaces in heptane:
(a) Symmetric asphaltene surfaces in heptane.
(b) Same system after 30 min waiting time

4.3.6 Adsorption kinetics experiments.

Asphaltene-toluene solutions of various asphaltene concentrations at 0.01 wt%, 0.1 wt%, 0.5 wt% and 1.0wt %, were prepared and injected in-between two mica surfaces to study the adsorption of asphaltene molecules onto mica. All the solutions were filtered using PTFE filters of 0.2 μm pore size (Millipore) before injecting. Figure 4.9 and Figure 4.10 show the approaching and separation force profiles of two mica surfaces in asphaltene in toluene solutions of three concentrations (0.01 wt%, 0.1 wt% and 1.0wt %) for different adsorption time. Continuous shifts in the hard wall thickness with time were observed for all cases. The hard wall thickness as a function of adsorption time summarized in Figure 4.11 shows a continuous adsorption and build-up of asphaltenes on mica surfaces.

For the lowest concentration of 0.01 wt% asphaltene in toluene solution, a hard wall thickness of ~12 nm was observed on the first approach (~5 min adsorption time), which corresponds to ~6 nm or a layer of asphaltenes on each mica surfaces. No significant further adsorption was observed during the first ~ 4 hours. The hard wall shifts out only from ~12 to ~17 nm. A significant adsorption was observed after ~20 hours, leading to a hard wall thickness of ~100 nm. With increasing solution concentration from 0.1 wt% to 1.0 wt%, the asphaltenes adsorbed onto the mica surface at a much faster rate. The hard wall thickness shifted to ~100 nm within ~1.5 hours in the 1.0 wt% solution, in contrast to ~12 nm in the 0.01 wt% solution.

Figure 4.9 (a)

Figure 4.9 (b)

Figure 4.9 Approaching surface force profiles of mica surfaces in asphaltene solutions of different concentrations and at different time intervals. All times are referenced to the instant when solution was injected between the surfaces.

(a) 0.01 wt % asphaltene in toluene solution

(b) 0.1 wt% asphaltene in toluene solution

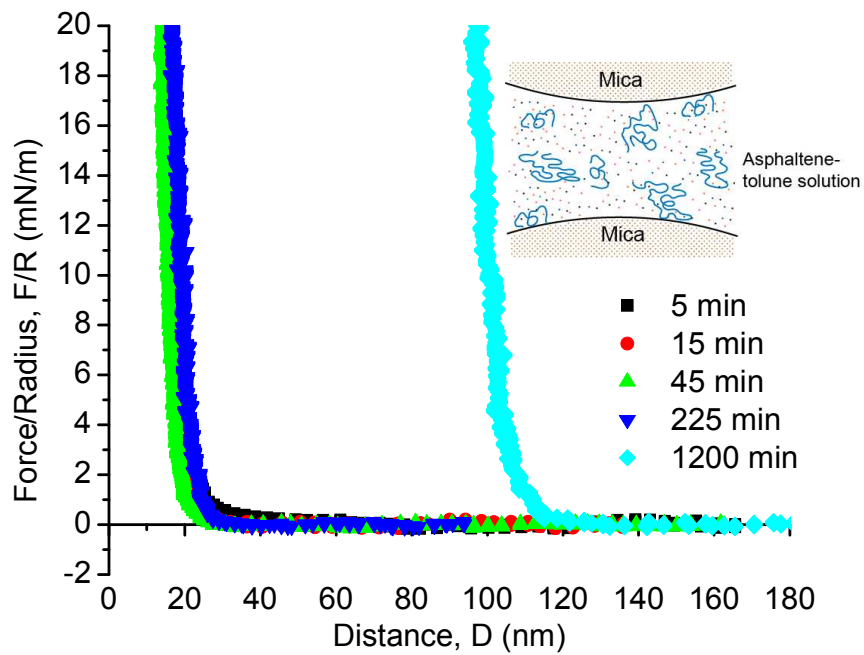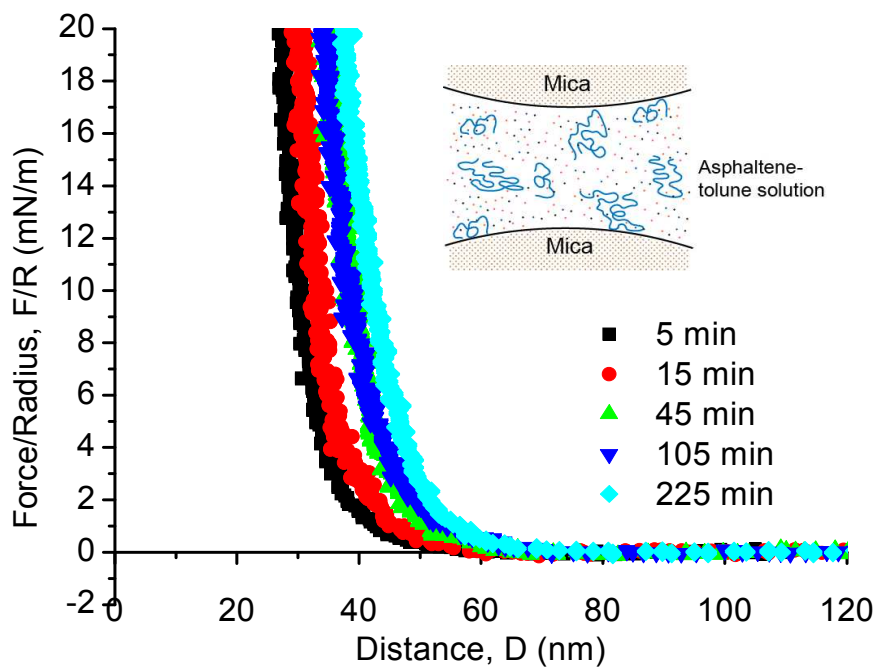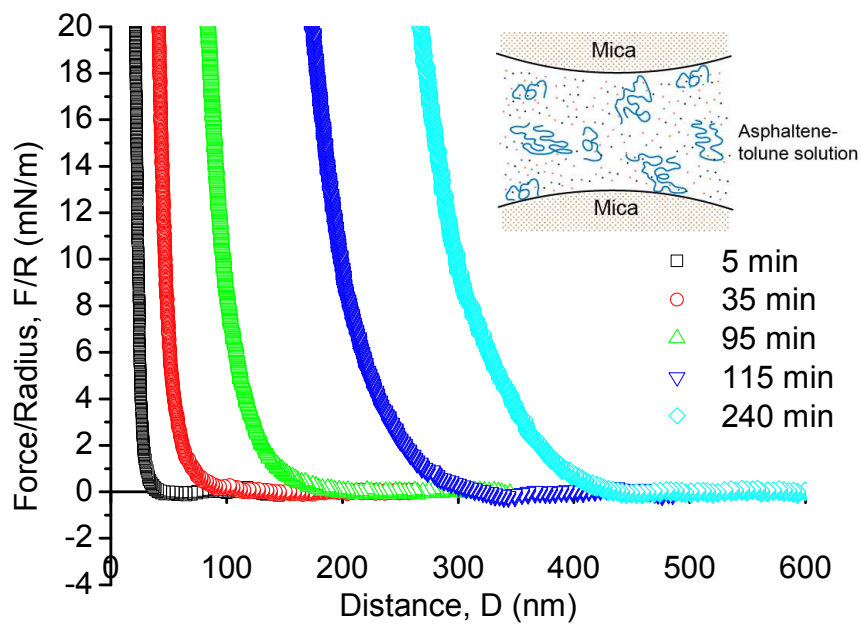(c) 1 wt% asphaltene in toluene solution.
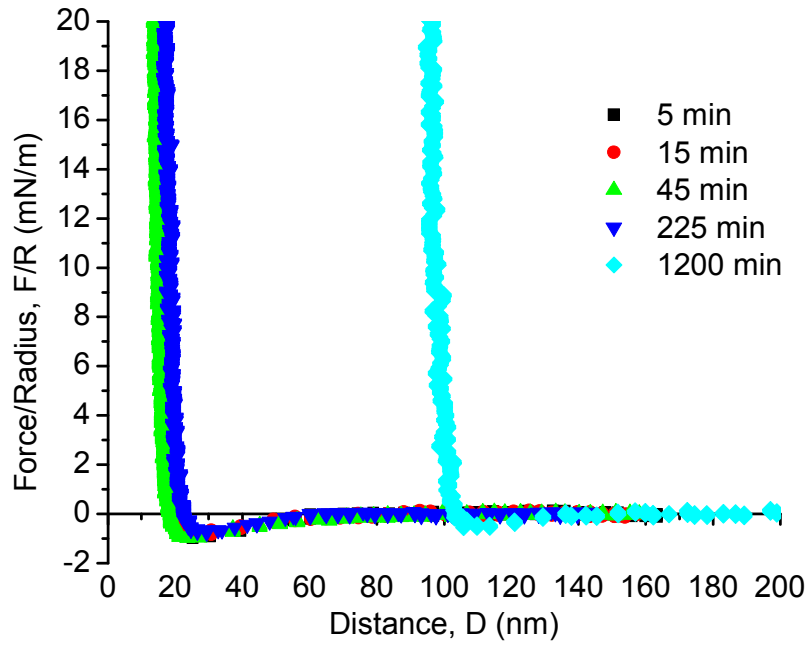
Figure 4.10 (a)

Figure 4.10 (b)

(c)
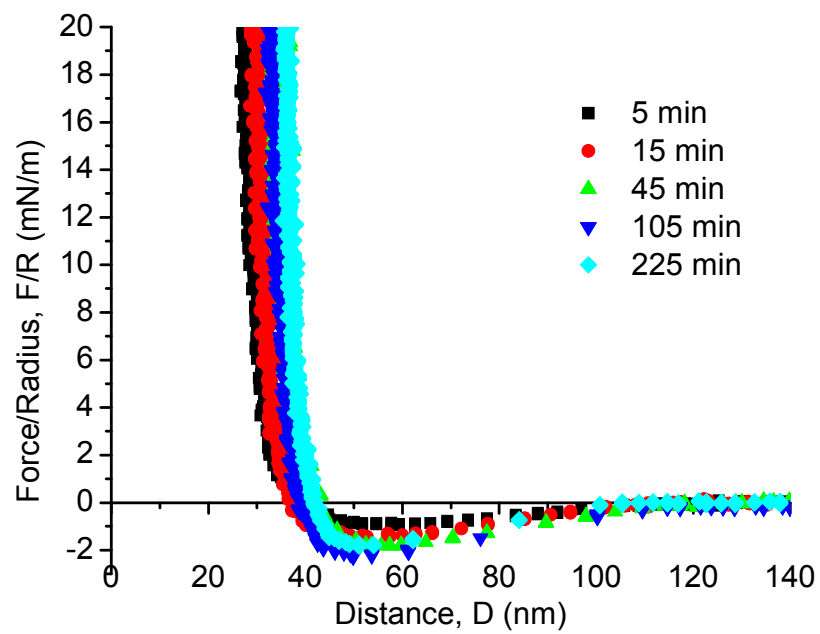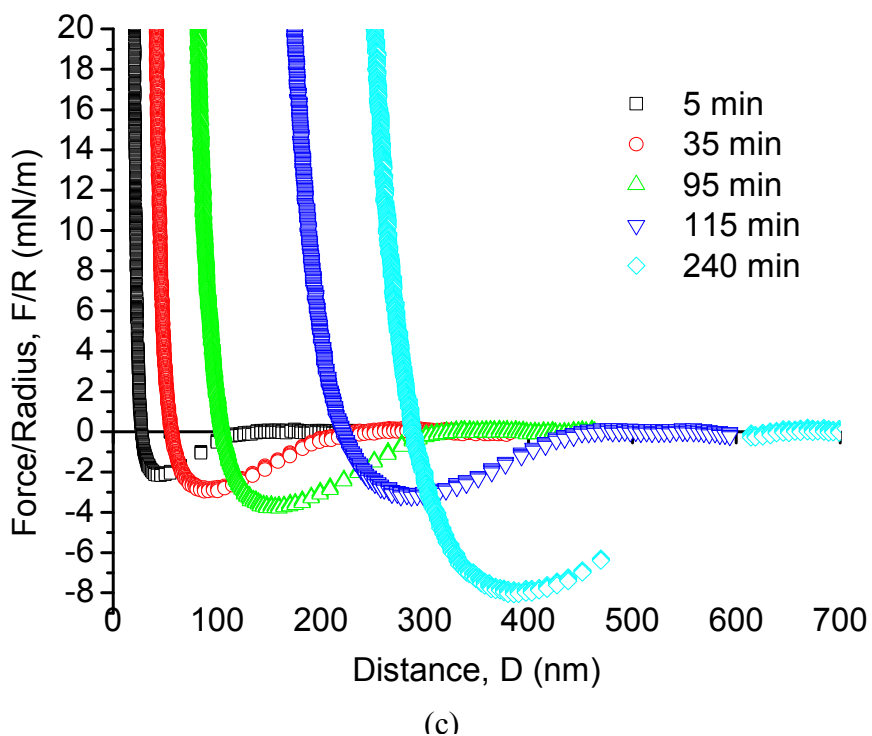
Figure 4.10 Retracting surface force profiles of mica surfaces in asphaltene solutions
of different concentration and at different time intervals.

(a) 0.01 wt % asphaltene in toluene solution

(b) 0.1 wt% asphaltene in toluene solution

(c) 1 wt% asphaltene in toluene solution.

Other interesting characteristics of the force profiles in Figure 4.9 and Figure 4.10 should

also be noted. (1) The repulsive forces become longer range with increasing the hard wall

thickness and adsorption time, which is evident for the 1.0wt% solution. The two

adsorbed asphaltene layers can be compressed and the gap between the two mica

surfaces, D decreases to ~20 nm hard wall up to 4 hours adsorption in the 1.0 wt% solution. The increase in hard wall thicknesses suggests adsorption of asphaltene aggregates on mica surfaces, and the increase in the range of repulsive force of the adsorbed layers is mainly attributed to the steric repulsion. (2) Strong adhesive forces are observed during the separation as shown in Figure 10a, b, and c. All the separation force profiles show that the asphaltenes are stretched before the two surfaces jump apart. For example, the asphaltene layers were stretched from 20 to >100 nm before they were separated, as shown in Figure 10c. The above results indicate several aspects of the adsorption mechanism of asphaltenes onto mica (one of the clay surfaces): (i) The asphaltenes have strong adhesion to mica in toluene, leading to interdigitation between two mica surfaces under compression; (ii) The adsorption of asphaltenes depends on time and solution concentrations; (iii) The adsorbed asphaltenes are soft and compressible, but asphaltene layer may not be smooth, which is supported by the long range repulsion and high compressibility of asphaltene layers, as shown in Figure 4.9 and 4.10. Figure 4.11 shows the relationship between hard wall thickness and the adsorption time for the asphaltene-toluene solutions of four concentrations. There is an increase in the hard wall thickness for all concentrations of asphaltene in solutions, but more significant at higher concentrations.

4.3.7 Stability of water-in-oil emulsions in bitumen production

Diluted bitumen during the bitumen production process still contains certain amount of water (2-3 wt%) and solids (0.5 wt%). The remaining water usually forms droplets in the continuous oil phase, which is highly undesirable. The presence of these solids and water could lead to serious processing problems such as equipment fouling and, and cause significant cost increase due to transportation difficulties and equipment corrosion. The stability of emulsions is directly related to the water-oil interface and interfacial properties. Our results in this study provide an insight into the interaction mechanisms of asphaltenes and clay surfaces in organic media and its relation to the stability of the water-in-oil emulsions.

The SFA measurements in this study show that two asphaltene surfaces have steric repulsion in toluene, while asphaltenes show strong adhesion to clay surfaces. With sufficient compression, adsorbed asphaltenes could interdigitate to induce adhesion between two clay surfaces. Our finding indicates that the fine solid/clay particles can have strong binding with asphaltenes in diluted bitumen. As asphaltenes are amphiphilic, the asphaltene and asphaltene-contaminated fine particle prefer to stay at the interface of water droplets and continuous organic phase, and form a semirigid interfacial film. The steric repulsion between the asphaltenes at two water/oil interfaces and the rigid interfacial film result in a strong energy barrier preventing water droplets from attaching to each other and coalescing. A schematic representation is shown in Figure 4.12.
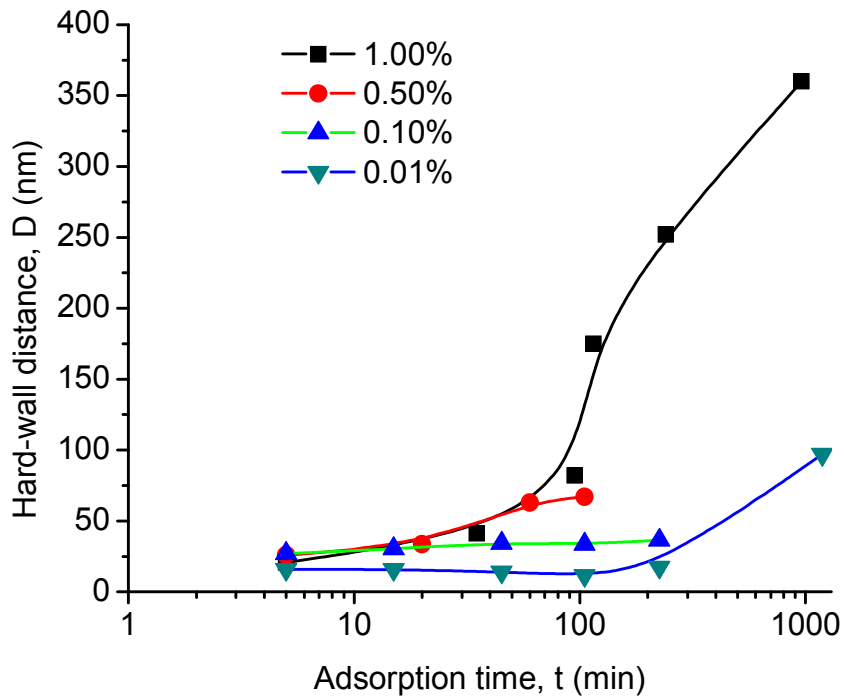
Figure 4.11 Hard wall distance vs adsorption time for different

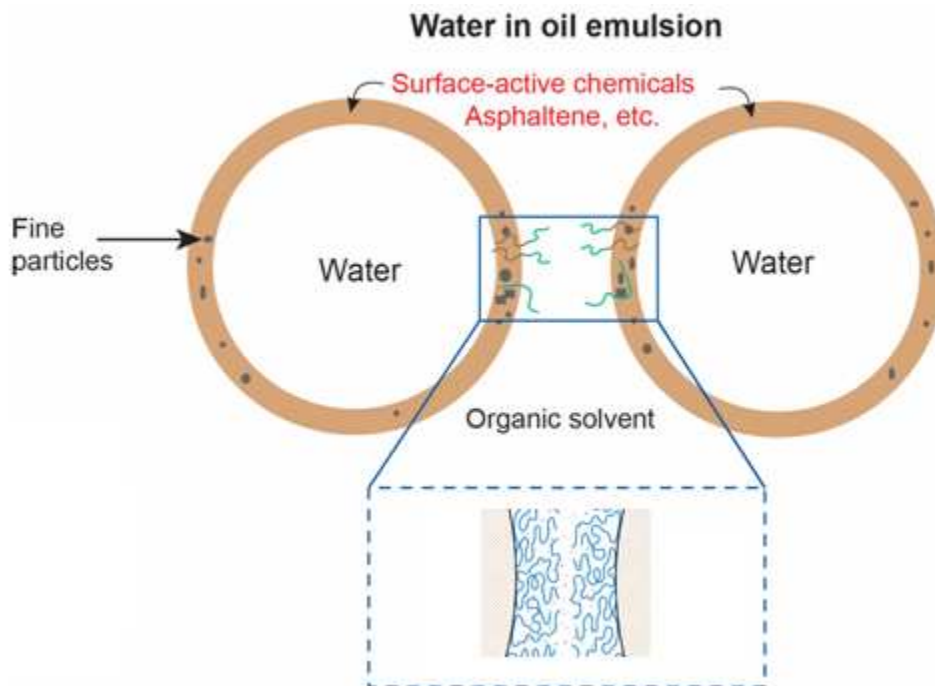concentrations of asphaltene solution (wt %).

Figure 4.12 Asphaltenes adsorbed at the interface prevent water from

coalescing and stabilize water in oil emulsions.

CHAPTER 5   SUMMARY AND CONCLUSIONS

The interactions between asphaltene surfaces in toluene and heptane were measured using a surface force apparatus. The SFA force measurements provide a direct evaluation on molecular interactions of asphaltenes in organic solvents, indicating explicitly the molecular aggregation, association, flocculation and adsorption of asphaltenes in toluene and heptane. AFM was used to obtain complimentary information on the morphology change of the asphaltene surfaces in organic solvents with time. Our results show that the surface interactions and adsorption kinetics of asphaltenes on solids strongly depend on types of surrounding solvents, contact time, load (pressure), concentrations of asphaltenes and and the nature of supporting substrates. Adhesion forces were measured between one asphaltene surface and one mica surface in both toluene and heptane, as well as between two asphaltene surfaces in heptane. Although small adhesion was observed for two asphaltene surfaces in toluene initially, pure repulsion was observed with increasing incubation time, which was mainly due to swelling and build up of adsorbed asphaltenes, causing steric repulsion. The AFM imaging of immobilized asphaltenes on solids, with soaking time in solvents, showed changes in conformation and morphology for dip-coated asphaltene thin films in toluene, but showed less change in heptane, which is in line with the results from the SFA force measurements. The adsorption of asphaltenes onto mica surface depends on time and concentrations of the solution. Asphaltenes can provide attractive bridging forces due to interdigitation of adsorbed asphaltenes between two mica surfaces. The steric repulsion between asphaltene surfaces in toluene and

adhesion between asphaltene and clay surfaces are considered to significantly contribute to the stability of the water-in-oil emulsions in bitumen and crude oil production. Future experiments are planned to reveal the intermolecular interaction mechanism between asphaltenes and different demulsifiers in organic solvents, which help disrupt the water-in-oil emulsions and remove the residue water in diluted bitumen.

CHAPTER 6   FUTURE WORK

This thesis work is a preliminary study of applying the advanced SFA technique to the oil sands research field. The asphaltene surfaces were deposited on mica substrates by dip coating. Spin coating and LB coating methods for preparing asphaltene surfaces should be investigated in future research to gain a better understanding of Asphaltene interactions under different surface conditions. Solvents play critical roles in these surface interactions. So far we have only investigated the interactions in toluene and heptane, other solvents and mixture of various solvents should be investigated to mimic real industry process. Temperature also has significant impact on the intermolecular and surface interactions of asphaltenes. The SFA 2000 has the capability to control the temperature during force measurement, thus the future research should utilize this feature to elucidate the temperature effect on the surface forces.

Other interesting studies can also be carried out with SFA. For example, the effect of demulsifier addition (adding polymers, such as ethyl cellulose into the solvent) on the surface forces of asphaltenes is very important for destabilization of the water-in-oil emulsions.

The other important feature of the SFA 2000 is that it allows friction and shearing force measurement. This feature is very useful for surface dynamic mechanism study. Further study using this feature may shed light on some complicated industry processes such as the colliding and friction between bitumen small droplets during bitumen separation.

CHAPTER 7   References

Alberta ERCB Year in Review, "Reserves, production, and deliveries", 2008.

Alig, G, "Control and characterization of thin films during confinement and shear", PhD thesis, University of California, Santa Barbara, (2007).

Butt, H.J., K.Graf and M. Kappl, Physics and chemistry of interfaces, Wiley, (2003).

De Gennes, P.G., "Polymers in an interface; A simplified view", Adv. Colloid Interface Sci., 27, 189-209, (1987).

Department of Energy, US, DOE/METC-86/2023, "In situ recovery of oil from Utah tar sand: A summary of tar sand research at the Laramie energy technology center", (1985).

Derjaguin, B., L Landau, "Theory of the stability of strongly charged lyophobic sols and of the adhesion of strongly charged particles in solutions of electrolytes", Acta Physico Chemica URSS, 14, 633-662, (1941).

Drelich, J. and J.D. Miller, "Surface and interfacial tension of the Whiterocks bitumen and its relationship to bitumen release from tar sands during hot water processing," Fuel, 73, 1504-1510 (1994).

Ducker, W.A., T.J. Senden and R.M. Pashley, "Direct measurement of colloidal forces using an atomic force microscope", Nature, 353, 239-241, (1991).

Ducker, W.A., T.J. Senden and R.M. Pashley, "Measurement of forces in liquids using a force microscope," Langmuir, 8, 1831-1836, (1992).

Grahame, D.C., "The electrical double layer and the theory of electrocapillarity", Chem. Rev., 41 (3), 441-501, (1947).

Heuberger, M, G. Luengo, J. Israelachvili, "Topographic information from multiple beam interferometry in the surface force apparatus", Langmuir, 13, 3839-3848, (1997).

Hunter, R.J., "Foundations of colloid science", 2nd ed, Oxford University Press, (2001).

Israelachvili, J.N., "Intermolecular and Surfaces Forces", 2nd ed. Academic Press, (1992).

Israelachvili, J.N., "Thin film studies using multiple-beam interferometry," J. Colloid Interface Sci., 44, 259-272, (1973).

Israelachvili, J.N. and G. E. Adams, "Measurement of forces between two mica surfaces in aqueous electrolyte solutions in the range 0-100nm," J. Chem. Soc. Faraday Trans. 1, 74, 975-1001, (1978).

Israelachvili, J.N., R. Pashley "The hydrophobic interaction is long range, decaying exponentially with distance", Nature, 300, 341-342 (1982).

Israelachvili, J.N., H. Wennerstroem, "Hydration or steric forces between amphiphilic surfaces? ", Langmuir, 6, 873-876, (1990).

Israelachvili, J.N., N. Alcantar, N. Maeda, T. Mates, M. Ruths, "Preparing contamination-free mica substrates for surface characterization, force measurement and imageing", Langmuir, 20, 3616-3622, (2004).

Klein, J., P. Luckham, "Forces between two adsorbed poly(ethylene oxide) layers immersed in a good aqueous solvent", Nature, 300, 429-431, (1982).

LeNeveu, D. M.; Rand, R. P.; Parsegian, V. A., "Measurement of forces between lecithin bilayers", Nature, 259, 601-603, (1976).

Lin, Q, "Interactions of bio-molecules and bio-surfaces", University of California, Santa Barbara, (2005).

Liu, J, Z. Xu, J. Masliyah, "Studies on bitumen –silica interaction in aqueous solutions by AFM", Langmuir, 19, 3911-3920, (2003).

Liu, J. "Role of colloidal interactions in bitumen recovery from oil sands," Thesis, University of Alberta, (2004).

Liu, J, Z. Xu, J. Masliyah, "Colloidal forces between surfaces in aqueous solutions measured with atomic force microscope", Colloids and Surfaces A: Physicochem. Eng. Aspects, 260, 217-228, (2005).

Long, J., L. Zhang, Z. Xu, and J.H. Masliyah, "Colloidal interactions between Langmuir−Blodgett bitumen films and fine solid particles", Langmuir, 22, 8831–8839, (2006).

Long, J., Z. Xu, and J.H. Masliyah, "Single molecule force spectroscopy of asphaltene aggregates", Langmuir, 23, 6182–6190, (2007).

Masliyah, J.H., "Fundamentals of oil sands extraction (ChE534 text book), University of Alberta, (2007).

Masliyah, J.H., and S. Bhattacharjee, "Electrokinetic and colloid transport phenomena", John Wiley & Sons, (2006).

McLean, J. D. and P. K. Kilpatrick, "Effects of asphaltene aggregation in model heptane–toluene mixtures on stability of water-in-oil emulsions", Journal of colloid and interface Sci., 196, 23–34 (1997).

Menon, V.B. and D.T. Wasan, "Particle-fluid interactions with application with to solid stabilized emulsions, Part I, The effect of the aspi-laltene adsorption", Colloids and Surfaces, 19, 89-105 (1986).

Meyer, E., "Complex interactions across aqueous solution", University of California, Santa Barbara, (2006).

Mullins, O. C., "Asphaltenes, heavy oils, and petroleomics" (2007).

Pashley, R. M., "Hydration forces between mica surfaces in aqueous electrolyte Solutions", J Colloid Interface Sci., 80, 153- 162, (1981).

Shelfantook, W., R. Tipman, N. Anderson, C. Strand, "Effect of alternate diluents in treatment of bitumen froth". CIM, Edmonton (1996).

Subramanian, M, "Supercritical fluid extraction of oil sand bitumens from the Uinta Basin, Utah", PhD Thesis, University of Utah, (1996).

Tadmor, R., N. Chen, J. Israelachvili, "Thickness and refractive index measurement using multiple beam interference fringes (FECO)", J. Colloidal and Interface Sci., 264, 548-553, (2003).

Tolansky, S., "Multiple-beam interferometry of surfaces and films", Oxford university press, (1949).

Verwey, E., J. Overbeek, "Theory of the stability of lyophobic colloids", Elsevier, Amsterdam (1948).

Vuillaume, K and S. Giasson, "Interactions between mica surfaces across crude oil and asphaltene solutions", J. Phys. Chem. C., 113, 3660-3665 (2009).

Wang S, J Liu, L. Zhang, Z. Xu, J. Masliyah, "Colloidal interactions between asphaltene surfaces in toluene", Energy & Fuel, 23, 862-869, (2009).

Wu, X., J. Czarnecki, N. Hamza, and J. Masliyah, "Interaction forces between bitumen droplets in water", Langmuir, 15, 5244-5250, (1999).

Yarranton, H. W., "Asphaltene solubility and asphaltene stabilized water-in-oil emulsions", PhD thesis, University of Alberta, (1997).

Yeung, A., Dabros, T., Masliyah, J. H., Czarnecki, J., "Micropipette: a new technique in emulsion research", Colloids and Surfaces A., 174, 169-181, (2000).

Zeng, H., "Interactions of polymer surfaces and thin films", PhD thesis, University of California, Santa Barbara, (2007).

Zhang, L, L. Steven, Z. Xu, and J. Masliyah, "Studies of athabasca asphaltene Langmuir films at air–water interface", J. Colloid Interface Sci., 264, 128-140, (2003).

Zhang, L, P. Breen, Z. Xu, and J. Masliyah, "Asphaltene films at a toluene/water interface", Energy & Fuels, 21, 274-285 (2007).

Zhao, H, J. Long, J.H.Masliyah, Z. Xu, "Effect of divalent cations and surfactants on silica-bitumen interactions", Industrial & Engineering Chemistry Research, 45(22), 7482-7490, (2006).